

Review

Recent Progress of Organic Photovoltaics with Efficiency over 17%

Xuelin Wang ¹ , Qianqian Sun ², Jinhua Gao ¹, Jian Wang ³, Chunyu Xu ¹, Xiaoling Ma ^{1,*} and Fujun Zhang ^{1,*}

¹ School of Science, Beijing Jiaotong University, Beijing 100044, China; 19121595@bjtu.edu.cn (X.W.); 18118027@bjtu.edu.cn (J.G.); 18121672@bjtu.edu.cn (C.X.)

² School of Physics and Electronics, Shandong Normal University, Jinan 250014, China; qianqiansun@sndu.edu.cn

³ College of Physics and Electronic Engineering, Taishan University, Taian 271021, China; wangjian@tsu.edu.cn

* Correspondence: maxl@bjtu.edu.cn (X.M.); fjzhang@bjtu.edu.cn (F.Z.)

Abstract: The power conversion efficiency (PCE) of organic photovoltaics (OPVs) has exceeded 18% with narrow bandgap, non-fullerene materials Y6 or its derivatives when used as an electron acceptor. The PCE improvement of OPVs is due to strong photon harvesting in near-infrared light range and low energy loss. Meanwhile, ternary strategy is commonly recognized as a convenient and efficient means to improve the PCE of OPVs. In this review article, typical donor and acceptor materials in prepared efficient OPVs are summarized. From the device engineering perspective, the typical research work on ternary strategy and tandem structure is introduced for understanding the device design and materials selection for preparing efficient OPVs.

Keywords: power conversion efficiency; organic photovoltaics; non-fullerene materials; ternary strategy; tandem structure



Citation: Wang, X.; Sun, Q.; Gao, J.; Wang, J.; Xu, C.; Ma, X.; Zhang, F. Recent Progress of Organic Photovoltaics with Efficiency over 17%. *Energies* **2021**, *14*, 4200. <https://doi.org/10.3390/en14144200>

Academic Editor: Marian Tzolov

Received: 31 May 2021

Accepted: 8 July 2021

Published: 12 July 2021

Publisher's Note: MDPI stays neutral with regard to jurisdictional claims in published maps and institutional affiliations.



Copyright: © 2021 by the authors. Licensee MDPI, Basel, Switzerland. This article is an open access article distributed under the terms and conditions of the Creative Commons Attribution (CC BY) license (<https://creativecommons.org/licenses/by/4.0/>).

1. Introduction

Environmental pollution and energy shortage have become the main issues restricting society development due to consumption of fossil fuels and excessive exploitation. In recent decades, increasingly more attention has been paid to environment friendly green energy, especially for solar energy, nuclear energy and wind energy [1,2]. Organic photovoltaics (OPVs) are developed to achieve the conversion from solar energy to electrical energy. Compared with inorganic photovoltaics, OPVs show unique advantages with blend donor and acceptor materials as solution-processed active layers. Solution-processed materials were synthesized in the form of colloidal semiconductor inks, as shown in Figure 1. Various methods could be used to form a solid film, such as spray coating, spin coating, inkjet printing, doctor blading or roll-to-roll printing [3]. Organic materials have some advantages, such as low-cost, large-area process ability, high absorption coefficients, tunable optical bandgap and energy levels [4,5]. After years of exploration, the device structure of OPVs has evolved from Schottky type to planar heterojunction type, and then to bulk heterojunction (BHJ) type. Currently, BHJ refers to the active layers formed by blending donor and acceptor materials. The donor and acceptor materials are interlaced with each other to form a bicontinuous interpenetrating network nanostructure [6,7]. Sufficient donor/acceptor interface is conducive to exciton dissociation, which strongly determines the performance of OPVs. Some efficient strategies were adopted to optimize phase separation of the active layer, such as solvent additives, thermal annealing treatment, solvent vapor annealing treatment and up-side-down post annealing treatments [8–11]. The active layer optimization method is commonly decided by the molecular structure of donor and acceptor materials. A dozen years ago, fullerene acceptor materials were used as the main acceptor materials of OPVs due to their good electron transport characteristics. Representative chemical structures of fullerene acceptors are shown in Figure 2. The blend of P3HT:PC₆₁BM was first

used as the active layer of OPVs, achieving a PCE of 2.8% [12]. However, the absorption of fullerene derivatives in the visible light region is relatively weak, and the tunability of the energy levels is limited. It is difficult to realize the breakthrough on the PCE of OPVs based on fullerene derivatives [13]. In contrast, non-fullerene acceptor (NFAs) materials possess readily adjustable energy levels and excellent characteristics on strong light absorption in the near-infrared region, which exhibit great potential in constructing highly efficient OPVs, especially for semitransparent OPVs [14,15]. In 2015, Zhan et al. developed ITIC based on a fused aromatic ring, and non-fullerene PSCs with medium bandgap conjugated polymer as the donor and ITIC as the acceptor had PCEs of 9–11% [16–18]. In 2019, Zou et al. designed a narrow bandgap NFA material Y6, leading to great improvement on PCE of binary OPVs [19]. Hereafter, a series of Y6 derivatives with narrow bandgap have been successfully designed and synthesized [20,21]. In 2021, a novel non-Y6 acceptor material named M3 was developed by Zheng et al. [22]. A 16.66% PCE is achieved in PM6:M3 based OPVs, which is comparable with Y6-series acceptor-based OPVs. Here, we summarize in Table 1 the typical works on OPVs with PCE over 17%, which exhibits great potential for the commercialization of OPVs as a green energy source.

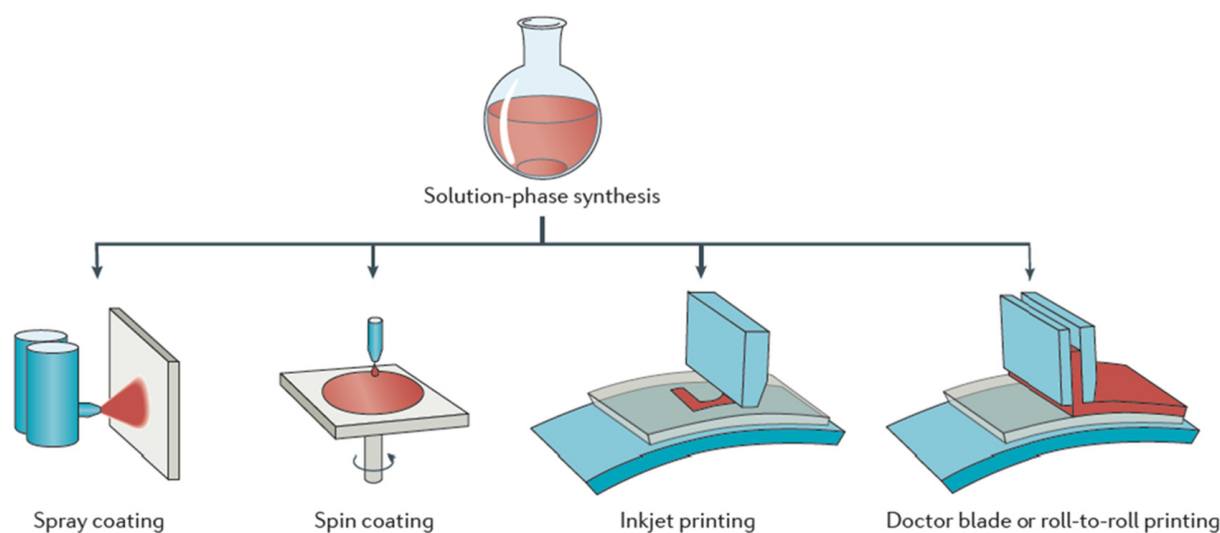


Figure 1. Different film preparation methods for solutions in the form of colloidal semiconductor inks. Reproduced from [3]. Reprinted with permission from ref. [3]. Copyright 2017 Nature Reviews Materials.

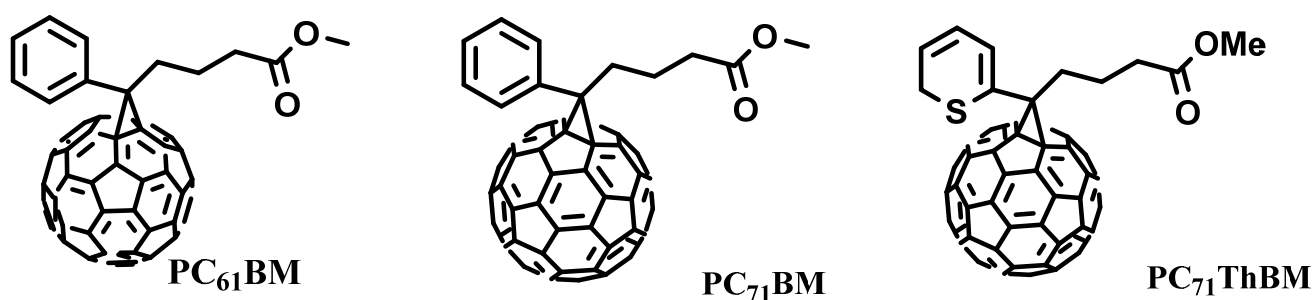


Figure 2. Representative chemical structures of fullerene derivatives.

In this review, we first introduce some BHJ materials including high-performance acceptors and donors. Next, we study the multicomponent-based OPVs that are mainly divided into ternary OPVs and quaternary OPVs. Then, we study OPVs and integrated perovskite/organic solar cells (IPOSs) in tandem OPVs. Finally, the application of the recent anode interface materials and cathode interface materials in the high efficiency organic solar cells is studied.

Table 1. The recent progress of OPVs with efficiency over than 17%.

Active Layer	Anode Modification Layer	Cathode Modification Layer	J_{SC} (mA cm ⁻²)	V_{OC} (V)	FF (%)	PCE (%)	Years	Ref.
PM6:BTP-4Cl-12	PP	PDINO	25.60	0.858	77.60	17.00	2019	[23]
PM7:Y6	PP	PNDIT-F3N	25.61	0.882	73.30	17.04	2020	[24]
PM6:BTP-2F-ThCl	PP	PNDIT-F3N	25.38	0.869	77.40	17.06	2020	[20]
PM6:Y6	PP	PDINN	25.89	0.847	78.59	17.23	2020	[25]
PM6-Ir1:Y6	PP	PNDIT-F3N-Br	26.12	0.845	78.41	17.24	2020	[26]
PM1:Y6	PP	PFN-Br	25.90	0.870	78.00	17.60	2020	[27]
PBQ6:Y6	PP	PDINN	26.58	0.851	77.91	17.62	2021	[28]
D18:Y6Se	PP	PNDIT-F3N-Br	27.98	0.839	75.30	17.70	2020	[29]
PM6:BTP-eC9	PP	PFN-Br	26.20	0.841	78.30	17.80	2020	[21]
D18:Y6	PP	PDIN	27.70	0.859	76.60	18.22	2020	[30]
PM6:L8-BO	PP	PNDIT-F3N-Br	25.72	0.870	81.50	18.32	2021	[31]
D18:N3	PP	PDIN	27.44	0.862	78.50	18.56	2021	[32]
PBDB-T-2F:Y6:PC ₇₁ BM	WS ₂	PFN-Br	26.00	0.840	78.00	17.00	2019	[33]
PM6:DRTB-T-C4:Y6	PP	PFN-Br	24.79	0.850	81.30	17.13	2020	[34]
PM6:Y6:PC ₇₁ BM	MoO ₃	ZnO	26.30	0.840	77.00	17.10	2020	[35]
PM6:Y6:PC ₇₁ BM	MoO ₃	OSiNDs	26.02	0.850	77.54	17.15	2020	[36]
PM6:PYT:PY2F-T	PP	PNDIT-F3N	25.20	0.900	76.00	17.20	2021	[37]
PM6:Y6:MF1	PP	PDIN	25.68	0.853	78.61	17.22	2020	[38]
PM6:BTP-4F-12:MeIC	PP	PDIN	25.40	0.863	79.20	17.40	2020	[39]
PM6:Y6:ITCPTC	PP	PNDIT-F3N	25.67	0.861	78.80	17.42	2020	[40]
PM6:Y6:BTP-S2	PP	PFN-Br	26.20	0.880	75.80	17.43	2020	[41]
PM6:Y6:C8-DTC	PP	PDINO	26.50	0.873	75.61	17.52	2020	[42]
PM6:S3:Y6	PP	PDIN	25.86	0.856	79.19	17.53	2020	[43]
PM6:BTP-4F-12:Y6-1O	PP	PDIN	26.13	0.860	78.26	17.59	2020	[44]
PM6:Y6-1O:PC ₇₁ BM	PP	PNDIT-F3N	24.90	0.900	78.50	17.60	2020	[45]
PM6:BTP-4F-12:IT-M	PP	PDIN	25.95	0.875	78.02	17.71	2021	[46]
D18-Cl:Y6:Y6-1O	PP	PDIN	25.87	0.900	76.92	17.91	2021	[47]
PM6:BTP-eC9:PC ₇₁ BM	PP	PFN-Br	26.93	0.856	79.40	18.30	2020	[48]
D18-Cl:N3:PC ₆₁ BM	PP	PDIN	28.22	0.849	78.00	18.69	2021	[49]
PM6:Y6:IDIC:PC ₇₁ BM	PP	PDINO	26.19	0.866	75.29	17.07	2020	[50]
PhI-Se:PM6:Y6:PC ₇₁ BM	PP	PDINO	26.30	0.851	76.80	17.20	2020	[51]
PM6:Y6:SR197:PC ₇₁ BM	MoO ₃	ZnO	27.11	0.841	76.62	17.48	2021	[52]
PM6:PTQ10:PC ₇₁ BM:N3	PP	PNDIT-F3N	26.78	0.852	77.70	17.73	2020	[53]
PM6:PM7:Y6:PC ₇₁ BM	PP	PFNDI-Br	26.55	0.859	79.23	18.07	2021	[54]

PP stands for PEDOT:PSS.

2. Efficient Donor and Acceptor Materials

In the past ten years, many novel NFAs have been designed, such as those based on a perylene diimide (PDI), naphthalene diimide (NDI) or benzothiadiazole (BT) core. Representative chemical structures of NFAs are shown in Figure 3. The bandgaps, energy levels, planarity and crystallinity characteristics of NFAs can be easily adjusted by chemical modification. Currently, most of the highly efficient OPVs are fabricated with narrow bandgap NFAs as acceptors and wide bandgap polymer as donors [20,21,23–27,29–32]. Zou et al. synthesized a new NFA Y6 exhibiting NIR absorption onset at 931 nm [19]. The 15.7% PCE was achieved when blending Y6 with PM6 as active layers, pushing the field of OPVs to a higher level. After that, the scientists focused on how to modify the Y6 molecule and design correspondingly new polymer donors. In 2019, Yao et al. reported a chlorinated NFA named BTP-4Cl by replacing the fluorine atoms on the terminal electron-withdrawing units of Y6 with chlorine atoms [55]. When blending with polymer donor PM6, BTP-4Cl based OPVs exhibit much higher V_{OC} of 0.867 V compared with that of the Y6 based OPVs (0.834 V). According to electroluminescence quantum efficiency ($E_{QE_{EL}}$) measurement of blend films, the BTP-4Cl based films exhibit a higher $E_{QE_{EL}}$ (3.47×10^{-4}) than that of BTP-4F based films (1.40×10^{-4}), resulting in reduced non-radiative loss of ~24 meV. A

PCE of 16.5% can be achieved, resulting from concurrently improved J_{SC} of 25.4 mA cm^{-2} and V_{OC} of 0.867 V. It should be noticed that the conjugation area of BTP-4Cl increases due to the substitution of fluorine by chlorine atoms, which leads to the poor solubility of BTP-4Cl. When the 0.81 cm^2 devices were fabricated by doctor blade coating means, the PCE of large area OPVs dramatically dropped to $10.7 \pm 0.5\%$, which should be mainly due to poor morphology of blend film caused by limited solubility of BTP-4Cl. To improve the process ability of BTP-4Cl, Yao et al. further prolonged alkyl chains of 2-ethylhexyl on pyrrole rings to 2-hexyldecyl and 2-butyloctyl [23]. A relatively high PCE of 17% could be achieved in the PM6:BTP-4Cl-12 based OPVs.

In addition to process ability of materials, the alkyl chains have important influences on intermolecular accumulation and charge transport. Ge et al. modified the alkyl side chains of Y6 and synthesized an NFA BTP-4F-12 [56], as shown in Figure 3. In comparison with Y6, the longer alkyl side chains of 2-butyloctyl were introduced to BTP-4F-12. Both Y6 and BTP-4F-12 show similar photon harvesting range and energy levels. The chemical property difference between Y6 and BTP-4F-12 is mainly decided by their molecular arrangement in solid films. The molecular ordering of neat NFA films is studied by using grazing incidence wide-angle X-ray scattering (GIWAXS) measurement. The BTP-4F-12 film has a narrower (100) peak than Y6, and a smaller full width at half-maximum (FWHM, Δq). The crystal coherence lengths (CCLs) of the (100) peaks are calculated as 56.5 and 35.3 Å for BTP-4F-12 and BTP-4F-8 films. As the lamellar stacking of the BTP-4F-12 is enhanced, charge transport ability can be improved in the corresponding blend films. All of the active layers were prepared by a spin-coating method with CF as processing solvent; PBDB-TF:BTP-4F-12 based OPVs exhibit a relatively high PCE of 16.4% in comparison with 15.3% of PM6:Y6 based OPVs. More noteworthy is that BTP-4F-12 dissolves better in some low-toxic solvents, such as 1,2,4-TMB, o-xylene and THF. The chemical structures of varied solvents are shown in Figure 4a. The polymer donor PBDB-TF-T1 with greater solubility was selected to replace PM6 as donor. The detailed PCEs of the OPV cells processed by different solvents are shown in Figure 4b. By employing THF as the processing solvent, a PCE of 16.1% can be achieved for the PBDB-TF-T1:BTP-4F-12 based OPVs, which is very close to that of OPVs fabricated with halogenated solvents. Furthermore, 1.07 cm^2 devices were fabricated by the spin-coating and blade-coating methods (Figure 4c), using THF as the processing solvent. As shown in Figure 4d, the resulting devices showed similar photovoltaic parameters. Impressively, a high PCE of 14.4% was still maintained in large-area OPVs with 1.07 cm^2 active area prepared by the blade-coating method. The results show that modifying the side chain can achieve the purpose of adjusting the processing ability of materials, and further achieve large-scale production in harmless solvents.

In addition to the central alkyl chains, there are two alkyl chains on the edge of the bithiophene units. In 2020, Yao et al. conducted optimization of alkyl chains on the edge of BTP-4Cl-BO (a Y6 derivative) and studied their applications in OPVs. The BTP-eC9 and BTP-eC7 were successively synthesized by shorting the n-undecyl to n-nonyl and then to n-heptyl [21]. Compared with BTP-BO-4Cl, BTP-eC9 has not only excellent solubility, but also enhanced molecule ordering. The better morphology features of PM6:BTP-eC9 blend films are beneficial to charge transport while inhibiting charge recombination. An outstanding PCE of 17.8% can be achieved in BTP-eC9 based OPVs, which should be the top levels in the field of OPVs at that time. The BTP-eC7 exhibits relatively low solubility and excessive aggregation in PM6:BTP-eC7 blend films, resulting in a slightly lower PCE of 14.9%. Optimizing the structure of Y6 derivatives with the same conjugated skeleton is conducive to exploring materials for manufacturing efficient OPVs.

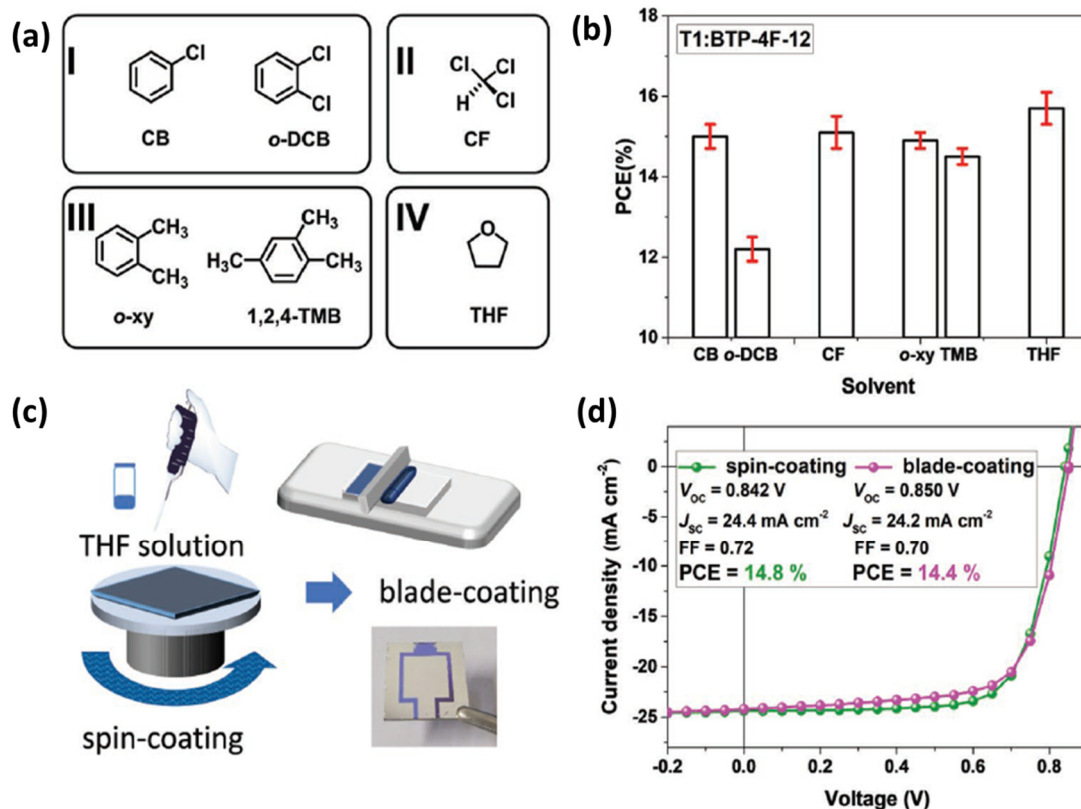


Figure 4. (a) Molecular formulas. (b) PCE histograms. (c) Schematics diagram of the spin-coating and blade-coating processes, and picture of the actual device. (d) The J - V curves of devices at a 1.07 cm² area. Reproduced from [55].

By improving the Y6 molecule, good chemical properties can be customized. In 2020, He et al. designed a dissymmetric fused-ring acceptor BTIC-2Cl- γ CF₃ with chlorine and trifluoromethyl end groups [57]. “When using PBDB-TF as a donor, the toluene-treated binary device achieved a high PCE of 16.31%, which was further increased to 17.12% when PC₇₁ThBM was added as the third component (J_{SC} of 25.7 mA cm⁻², V_{OC} of 0.85 V and FF of 78.10%).” [57]. Among polymer solar cells treated with non-halogenated solvents, a PCE of more than 17% is the highest on record. In 2021, Sun et al. synthesized a highly efficient non-fullerene acceptor L8-BO by substituting the beta position of the thiophene unit on a Y6 based dithienothiophen[3,2-b]-pyrrolobenzothiadiazole core with branched alkyl chains [31]. The PM6:L8-BO based ternary OPVs achieved a high PCE of 18.32% (certified value of 17.9%), V_{OC} of 0.874 V, J_{SC} of 25.72 mA cm⁻² and FF of 81.5%. The emergence of high efficiency Y6 derivatives provides the possibility to achieve higher efficiency OPVs.

Compared with the emerging NFAs, high-performance donors matching those low-bandgap NFAs are still few. A series of typical donors have been synthesized, such as PBDB-T, PTB7-Th, PM6, PM7 and others. Representative chemical structures of polymer donors are shown in Figure 5. Hou et al. reported a D-A type copolymer PM6 in 2015. The introduction of BDT-F units can effectively lower the highest occupied molecular orbital (HOMO) and the LUMO levels of materials, leading to improved photovoltaic performance. Unfortunately, synthesis cost of the OPV materials containing fluorine is very high [58,59]. In 2018, Hou et al. further modified PM6, chlorinated the side groups of thiophene and synthesized a new copolymer PM7 with a similar chemical structure [60]. Compared with fluorinated polymers, the chlorinated polymers have obviously lower synthesis cost and similar optoelectronic properties. The relatively low HOMO level of PM7 is helpful for improving V_{OC} of the resulting OPVs. The two polymers (PM6 and PM7) were blended with IT-4F to fabricate OPVs under the same preparation conditions. The PM6:IT-4F based OPVs exhibited a PCE of 13.2%, with J_{SC} 20.81 mA cm⁻², V_{OC} 0.84 V and FF of 76%. The PM7:IT-4F based OPVs showed a higher PCE of 14.4%, with J_{SC} of 21.80 mA cm⁻², V_{OC} of

0.86 V and FF of 77%. The result demonstrates that introducing chlorine into appropriate substituent positions is an effective strategy for preparing an efficient polymer donor. In 2019, Huang et al. synthesized a new D-A copolymer (P2F-EHp) in which deep HOMO level is achieved by a strong electron-withdrawing difluorophenyl group [61]. A PCE of 16.02% can be achieved in devices based on P2F-EHp:BTPPT-4F, benefiting from J_{SC} of 26.68 mA cm⁻², V_{OC} of 0.81 V and FF of 74.11%.

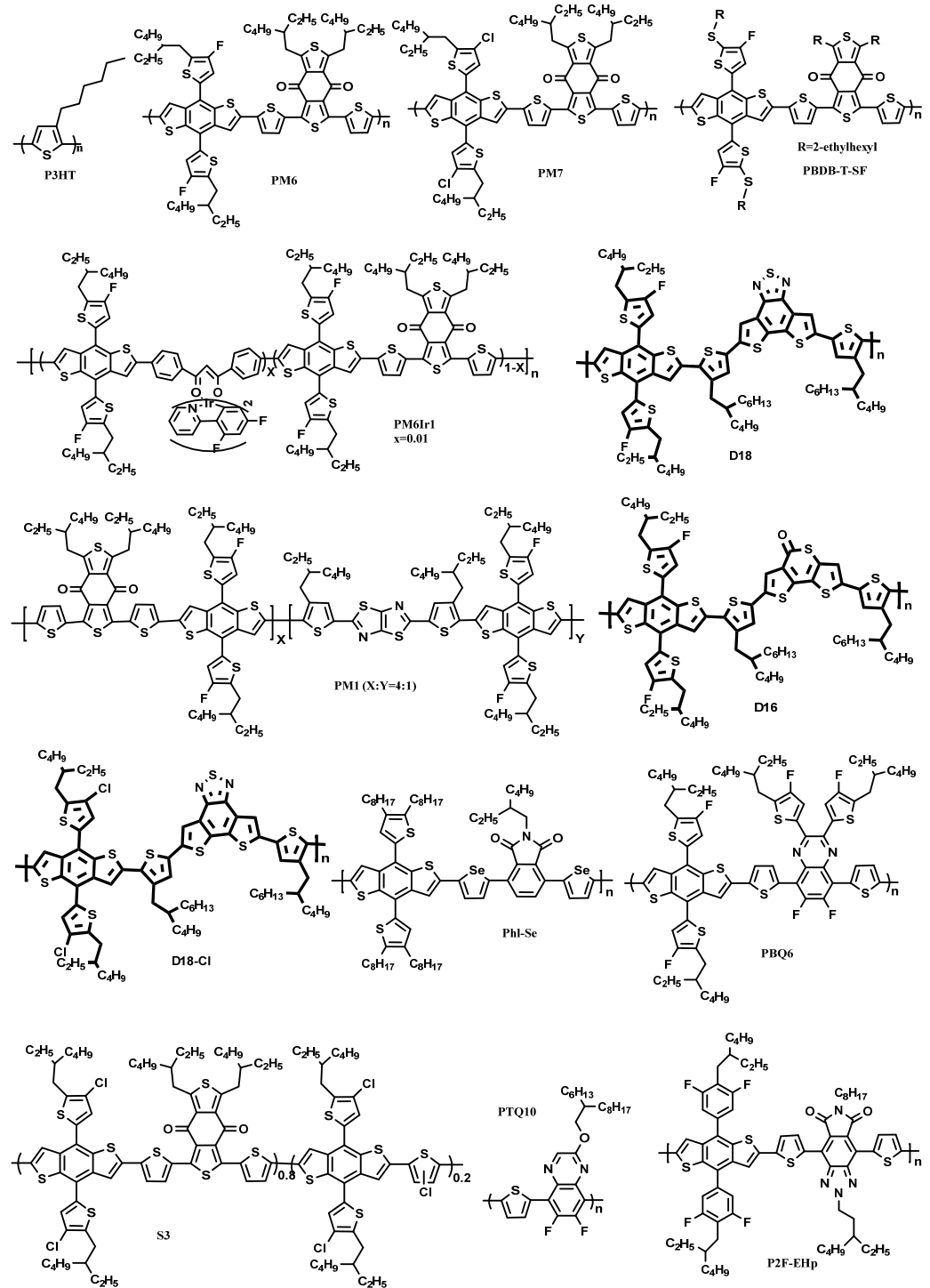


Figure 5. Representative chemical structures of polymer donors.

There is a great mission for the field to develop more high-performance donors that are well matched with NFAs. In 2019, Ding et al. synthesized D16 based on a fused-ring

thiolactone unit, 5H-dithieno[3,2-b:20,30-d]thiopyran-5-one (DTTP) [62]. These units have strong electron-withdrawing capability and extended molecular planes, giving copolymers deep HOMO levels, high hole mobility and enhanced π - π stacking. A PCE of 16.72% can be achieved in D16:Y6 based OPVs. In 2020, Ding et al. further modified D16 and synthesized D18 by using a fused-ring acceptor unit, dithieno[3',2':3,4;2'',3'':5,6]benzo [1,2,5]thiadiazole (DTBT) [30]. In comparison with DTTP, DTBT has a larger molecular plane, which gives D18 a higher hole mobility of $1.59 \times 10^{-3} \text{ cm}^2 \text{ V}^{-1} \text{ s}^{-1}$. A high PCE of 18.22% (certified 17.6%) can be achieved in D18:Y6 based OPVs, which should be one of the highest PCE of OPVs.

Incorporating suitable units into the polymer backbone has been proven to be an effective means to improve the microstructure of blend films. Based on this concept, a platinum (II) complexation strategy was developed by Peng et al. in 2019. A wide-bandgap copolymer PSFTZ was designed and synthesized based on benzodithiophene (BDT) donor unit and polynitrogen heterocyclic s-tetrazine (s-TZ) acceptor block [63]. PSFTZ exhibits a wide bandgap of 1.93 eV and a low-lying HOMO level of -5.50 eV , which matched well with efficient NFA Y6. The small HOMO level offset of 0.15 eV between PSFTZ and Y6 enabled a relatively low E_{loss} of 0.53 eV. Due to the strong aggregation characteristics of PSFTZ, the phase separation of this active layer was relatively large, which was not conducive to the exciton dissociation and increased the probability of charge recombination. The PSFTZ:Y6 based OPVs show a relatively low PCE of 13.03%, with J_{SC} of 25.10 mA cm^{-2} , FF of 64.9% and V_{OC} of 0.80 V. In order to study the effect of Pt complexation on crystallinity and molecular packing behavior, 2D-GIWAXS measurements were performed on polymer films with different Pt-complexation degrees, as shown in Figure 6. The coherent length (L_C) based on the (100) diffraction peak is gradually reduced from 131 \AA^{-1} to 95 \AA^{-1} along with the increase of the Pt-complexation degree. The intensity of (200) and (300) diffractions were simultaneously lowered with increasing the Pt-complexation degree. From the GIWAXS measurement, the introduction of platinum(II) complexation strategy can effectively inhibit the aggregation tendency of the polymer. When a certain amount of $\text{Pt(Ph)}_2(\text{DMSO})_2$ was added, organometallic complexation could occur between the $\text{Pt(Ph)}_2(\text{DMSO})_2$ and PSFTZ. Due to the steric hindrance of the benzene ring to the platinum complex, the aggregation strength of the polymer is suppressed, and the phase separation and film morphology are improved. The optimal PCE is significantly improved from 13.03% to 16.35% by adding 10% (molar ratio related to the s-TZ block) $\text{Pt(Ph)}_2(\text{DMSO})_2$, with enhanced J_{SC} of 26.45 mA cm^{-2} and FF of 76.3%. In 2020, Min et al. further developed highly efficient polymer donor materials based on a similar strategy. Different concentrations of iridium (Ir) complexes (0, 0.5, 1, 2.5 and 5 mol%; $(\text{dfppy})_2\text{IrdbmBr}$) were introduced into the polymer conjugated backbone of the commercially available polymer PM6 [26]. A series of OPVs were fabricated with PM6-Irx ($x = 0, 0.5, 1, 2.5$ and 5):Y6 as active layers. The addition of iridium (Ir) complexes into the PM6 can effectively improve BHJ morphology and simultaneously facilitate charge generation, accelerate carrier extraction and hinder carrier recombination. The optimal PCE of 17.24% can be achieved by adding 1 mol% of $(\text{dfppy})_2\text{IrdbmBr}$ unit, with simultaneously enhanced V_{OC} , J_{SC} and FF of 0.845 V, 26.12 mA cm^{-2} and 78.41%, respectively.

In recent years, more PM6 derivatives with excellent performance have been designed and synthesized to achieve higher efficiency OPVs. In 2020, Zhang et al. synthesized a donor polymer (named PM1) by including 20% weakly electron-withdrawing thiophene-thiazolothiazole (TTz) in the PM6 polymer backbone [27]. The PM1:Y6 based OPVs can achieve high PCE of 17.6%, J_{SC} of 25.9 mA cm^{-2} , V_{OC} of 0.87 V and FF of 78%. Excitingly, PM1 polymer has excellent batch-to-batch reproducibility compared to PM6, which is expected to become the main material of the non-fullerene OPV community. In 2021, Li et al. synthesized a D-A copolymer (PBQ6), which is based on biphenyl-benzodithiophene (BDTT) as the donor (D) unit and difluoroquinoxaline (DFQ) with two alkyl-substituted fluorothiophene side chains as the acceptor (A), and thiophene as the π -bridges [28]. The mixed film of PBQ6:Y6 showed more balanced hole/electron mobility, less charge

carrier recombination and a more favorable morphology compared with the mixed film of PBQ5:Y6. Therefore, the OPVs based on PBQ6:Y6 achieved a high PCE of 17.62% (J_{SC} of 26.58 mA cm^{-2} , V_{OC} of 0.851 V and FF of 77.91%), which is one of the highest PCE of binary OPV with polymer donor and Y6 acceptor. The emergence of multifarious donors provides the possibility of achieving higher efficiency OPVs.

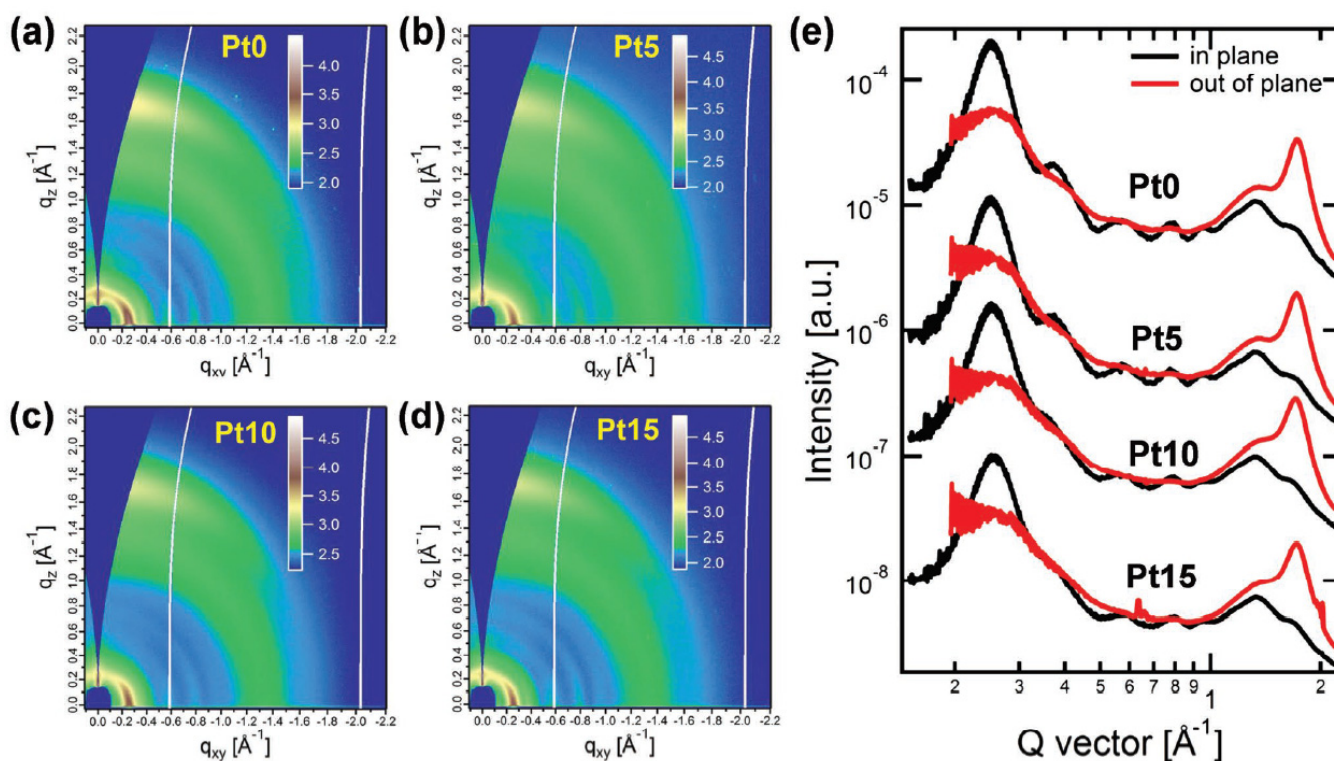


Figure 6. (a–d) The 2D-GIWXAS patterns. (e) IP and OOP line-cut profiles. Reproduced from [63]. Reprinted with permission from ref. [63]. Copyright 2019 Wiley.

3. Device Architecture

Single-junction OPVs have made great progress, mostly due to the complementary absorption spectra, matched energy levels and good compatibility of NFA and polymer donors [64,65]. It is well recognized that the absorption spectrum of organic materials is relatively narrow, which restricts the photon capture range of the multielement blend film. Enhanced photon capture ability of the active layer is the first step to achieve high efficiency OPVs [66–68]. It is found that if the width of the absorption window is doubled, PCE of OPV may be greatly improved [69]. Obviously, the active layer containing multiple components with complementary absorption spectra not only enhances photon capture, but also maintains a simple manufacturing process [70,71]. In addition, the introduced third or fourth component provides a variety of functions for the improvement of OPV performance, such as enhancing photon capture, optimizing distribution of photogenerated excitons, altering molecular arrangement and optimizing phase separation degree [72–74]. The important photovoltaic parameters of OPVs can be optimized to the maximum simultaneously or individually by incorporating appropriate third or fourth components as a photon harvesting enhancer and morphology regulator. Alternatively, in comparison with single-junction configuration, tandem OPVs can not only expand the photon absorption range and enhance the photon absorption intensity, but also decrease heat loss by stacking multiple subcells with different absorption ranges [75]. In fact, several technological challenges must be accurately controlled to fabricate high performance tandem OPVs, such as active layer thickness of each subcell, transmission and charge carrier collection ability of intermediate cathode, and the complementarities of active layer absorption spectra in each

subcell. Multicomponents and tandem strategy have been proven to be an efficient method to achieve performance improvement of OPVs. In addition, the development of interface engineering is also crucial to the preparation of high efficiency OPVs. The interface layers between organic active layers and electrodes play a vital role in determining the charge extraction dynamic process, which is closely related to FF of OPVs. PEDOT:PSS and PDIN are commonly employed as a hole transport intermediate layer (HTL) and the electron transport intermediate layer (ETL) [76,77] due to their considerable charge transport capabilities and appropriate energy levels. Currently, considerable effort has been expended to develop various ETLs and HTLs materials for achieving OPVs with better performance.

3.1. Multicomponent OPVs with BHJ Structure

To date, the reported multicomponent-based OPVs can be divided into ternary OPVs and quaternary OPVs, which contain three and four components in active layers, respectively. On the basis of the role of the third component, ternary OPVs can be classified into two categories: one donor/two acceptors and two donors/one acceptor. In quaternary OPVs, the third and fourth component may play different roles in improving the performance of OPVs. The active layer morphology in the quaternary system is more complicated compared with binary or ternary OPVs. Generally, materials with complementary absorption spectra are selected to achieve the purpose of covering a wider photon collection range in the active layer [70,78]. In addition, whether the materials have similar energy levels also needs to be considered. The similar LUMO or HOMO levels of multiple donors or acceptors can prevent the formation of deep charge trapping, thereby allowing better charge transfer in multicomponent-based active layers [79,80]. At the same time, good compatibility between multiple components is beneficial for the morphology of active layers, which is a factor worth considering. Many articles have shown that donors or acceptors with similar molecular structures often have good compatibility [81,82]. In addition, the complementary photovoltaic parameters are important criteria for the manufacture of high efficiency ternary OPVs [42,83]. The appearance of versatile donor and acceptor will make the development of ternary OPVs more rapid and flexible.

3.1.1. Working Mechanism in Multicomponents OPVs

At present, there are four working mechanisms in multiple OPVs: energy transfer, charge transfer, alloy model and parallel-linkage [69]. Taking ternary dual donor system as an example, the working mechanism of a multicomponent system is introduced. The position of the third component in the active layer is closely related to the working mechanism of multicomponent-based OPVs, which is decided by the phase structure and energetics of the third component. As shown in Figure 7a, the third component might (i) be directly embedded into donor, (ii) form its own transport channels, (iii) locate at the interface of donor and acceptor or (iv) form an alloy state with the main donor [84]. For the charge transfer mechanism (Figure 7b), corresponding LUMO and HOMO energy levels of D2 are between those of A1 and D1. The third component should act as a bridge for facilitating the transport of holes to the anode and electrons to the cathode [85]. Energy transfer (Figure 7c) should be a competing process in comparison with the charge transfer among the materials. The charge transfer and energy transfer can occur simultaneously in blend films, but only one working mechanism is dominant. Efficient energy transfer requires substantial overlap between the emission spectrum of one component and the absorption spectrum of another component, as well as <10 nm spacing between them. The energy transfer should provide a potential pathway to improve the utilization of excitons [86,87]. To explain the varied V_{OC} of ternary OPVs along with the addition of third component, the parallel-linkage (Figure 7d) and alloy model (Figure 5e) were proposed. In the case of the parallel-linkage, ternary OPVs are similar to the parallel connections between subcells in a tandem architecture. Excitons generated in the donor migrate to the corresponding donor/acceptor interface and decompose into free electrons and holes. Electrons are transported through the corresponding acceptor matrix to the cathode, and holes are transported to the an-

ode through a transport channel formed by the donor. There is no electronic interaction between two donors [88]. In the case of the alloy model, two donors are coupled into a new charge transfer state, which is determined by blend composition. Good compatibility among the materials used is generally required for the formation of the alloy model [38,89].

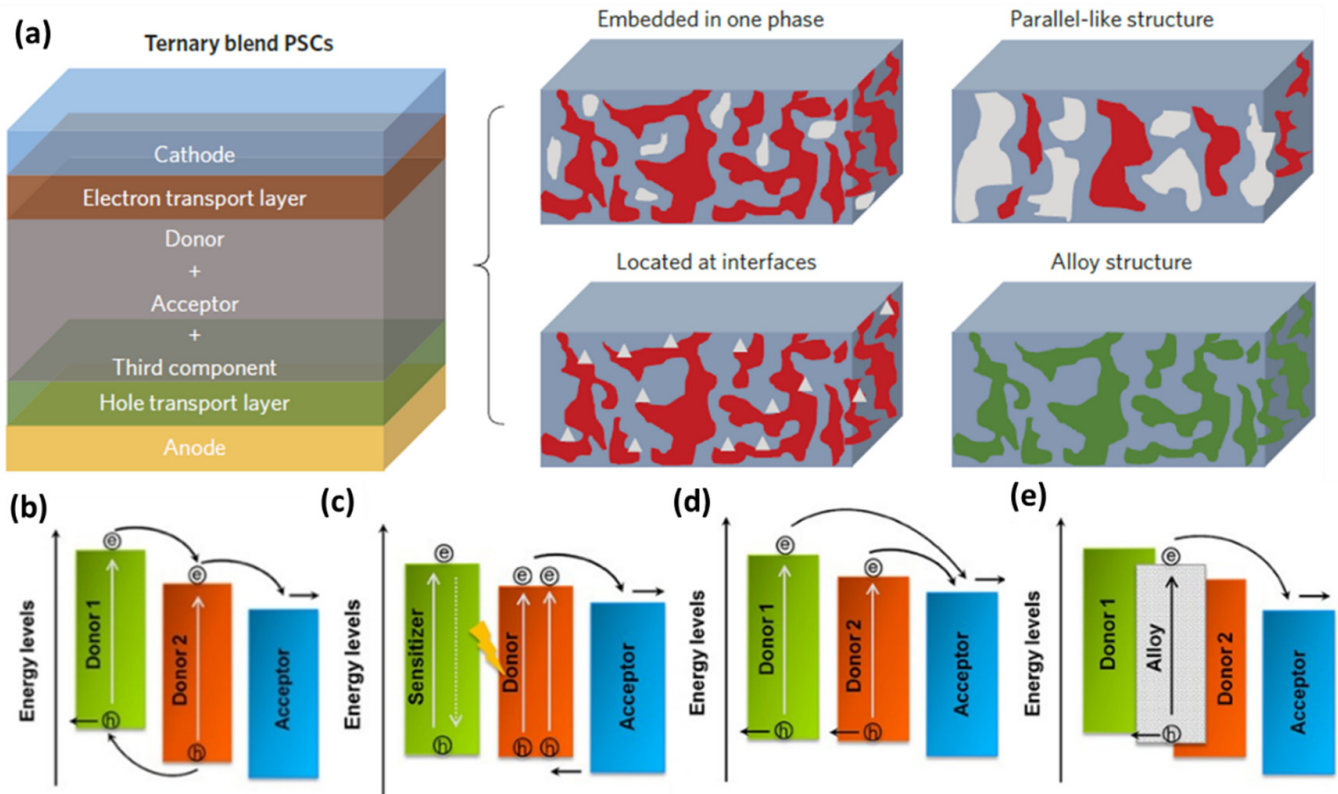


Figure 7. (a) Structures of ternary OPVs with four distribution patterns of the third component. Reproduced from [84]. Working principle diagram of ternary OPV based on double donors: (b) charge transfer, (c) energy transfer, (d) parallel-like mechanism and (e) alloy model. Reproduced from [90]. Reprinted with permission from ref. [84]. Copyright 2015 Nature Photonics; Reprinted with permission from ref. [90]. Copyright 2017 Wiley.

Recently, it was demonstrated that the proposed working mechanism can coexist in ternary OPVs. Different working mechanisms may be converted to each other along with varied content of active layer materials. Photoluminescence (PL) spectra, time-resolved transient photoluminescence (TRPL) spectra, J - V curves based on neat donor or acceptor devices and cyclic voltammetry (CV) curves should be popular and convenient tools to investigate and distinguish the corresponding working mechanism in ternary OPVs [91–93]. It was demonstrated that the distribution of the third component plays a vital role in determining the working mechanism of ternary OPVs. Recently, Zhang et al. proposed a new method to investigate compatibility among the used materials. In a PBDB-T-2Cl:Y6:PC₇₁BM based system, the characteristic Raman peaks of Y6, PBDB-T-2Cl and PC₇₁BM are 2219, 2960, and 259 cm⁻¹, as shown in Figure 8a. Raman map of blend films can be drawn based on the Raman characteristic peak of required material, as shown in Figure 8b [94]. The blue, green and red areas correspond to Y6, PC₇₁BM and PBDB-T-2Cl, respectively. According to the Raman images of the ternary blend film, most of the green dots are surrounded by blue dots, which reflect that PC₇₁BM tends to mix with Y6, between the two materials. Raman technology has been applied in other ternary systems, such as PM6:Y6:MF1 [38] and PM6:IT-2F:T6Me [95], which can give intuitive evidence on the compatibility of the materials.

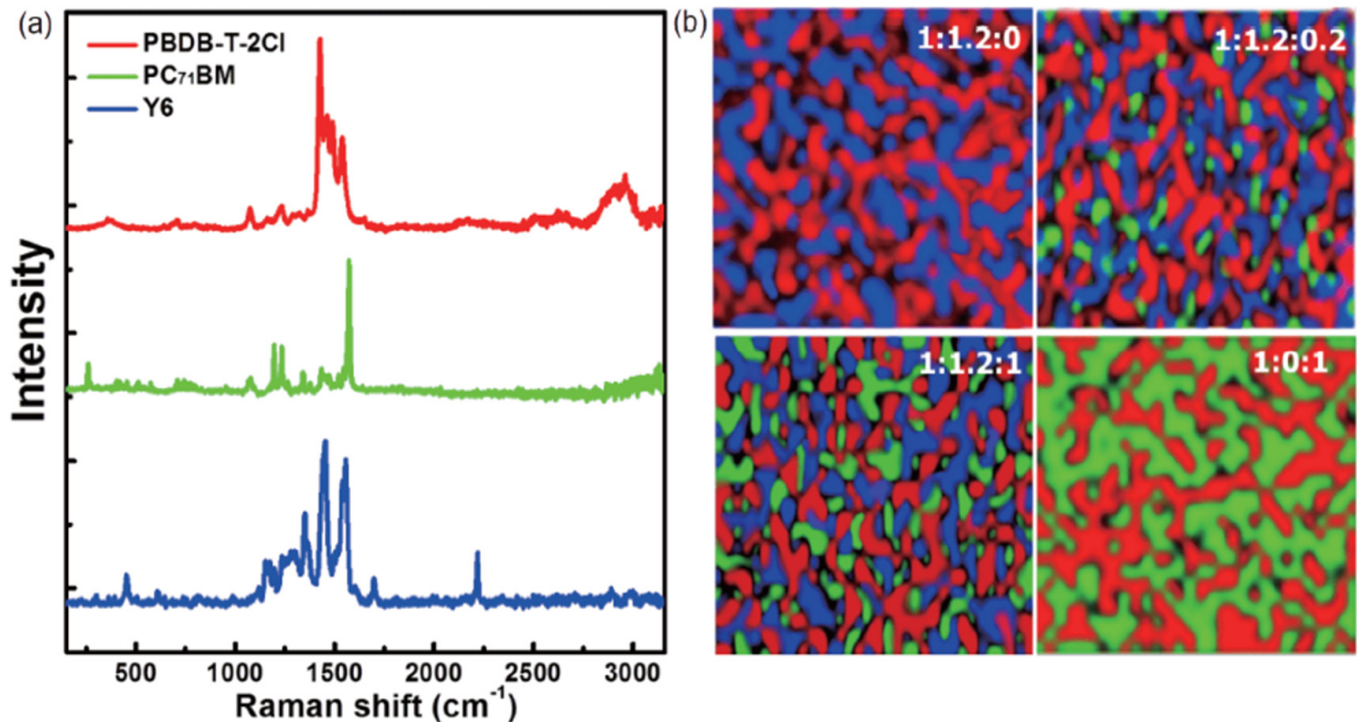


Figure 8. (a) Raman spectra of three materials: PBDB-T-2Cl, PC₇₁BM and Y6; (b) Raman mapping image of ternary blend films with different PC₇₁BM contents. Reproduced from [94]. Reprinted with permission from ref. [94]. Copyright 2019 Science China Chemistry.

3.1.2. Typical Works on Ternary OPVs

The combination of fullerene and NFAs is an efficacious means of selecting materials for fabricating ternary OPVs. In the past ten or more years, fullerene derivatives such as PC₇₁BM or PC₆₁BM have been extensively used as the acceptor for OPVs due to their advantages of large electron affinity, high electron mobility and anisotropic charge transport. On the contrary, fullerene derivatives have some disadvantages, such as the mismatched energy level and feeble absorption capacity with the donor, which leads to inadequate photon capture and odd voltage loss. In recent years, various NFAs have been designed and synthesized to fabricate OPVs due to their advantages of strong absorptivity in a particular range, low energy loss and tunable energy levels. In contrast, some blended films based on non-fullerene materials have large phase separation due to the strong crystallinity of NFAs. The association of fullerene and non-fullerene materials can actively solve the problem of poor morphology. Merits of fullerene and non-fullerene materials can be integrated into one cell through ternary strategy and result in performance preferable to that of OPVs based on an individual acceptor. The morphology and photon capture of active layers can be improved by mixing fullerene derivatives into a highly efficient binary system. In 2019, PC₇₁BM was incorporated into PM6:Y6 system by Peng et al. “A PCE of 16.67% is realized in the optimized ternary OPVs with the weight ratio of PM6:Y6:PC₇₁BM as 1:1.0:0.2.” [96]. Obviously, the intensity of EQE spectra in the absorption range 300–500 nm is simultaneously increased along with the increase of PC₇₁BM in acceptors, owing to enhanced photon capture by incorporating PC₇₁BM. Except for photon capture, the fullerene derivatives can also play the part of a morphology regulator for preferable charge transport and exciton dissociation in active layers. In 2020, Zhang et al. reported ternary OPVs with PM7:Y6:PC₇₁BM as the active layer. “The EQE of ternary OPVs are almost impossibly enhanced in the strong absorption spectrum range of PC₇₁BM, indicating that extra PC₇₁BM has negligible contribution on photon harvesting in the short wavelength range.” [94]. To investigate the influence of extra PC₇₁BM on morphology, GIWAXS and GISAXS characterizations were carried out. “The OOP (010) peak and IP

(100) peak can be concurrently enhanced in the PM7:Y6:PC₇₁BM (1:1.2:0.2, wt/wt) blend films, indicating the face-on orientation is more ordered in the optimum ternary blend films." [94]. There is, to emphasize, an IP (100) peak that is lightly shifted toward high q values in pace with more addition of PC₇₁BM, meaning lamellar staking spacing gets closer in optimized ternary OPVs. The improved molecular arrangement can facilitate charge transport in active layers. On the basis of GISAXS of hybrid films, the domain size of donor and acceptor can be calculated. The domain sizes of acceptor and donors can be well regulated by mixing added PC₇₁BM. For ternary hybrid films, analogous domain size of acceptor and donors approach the exciton diffusion length of about 10 nm, which is beneficial for efficient exciton dissociation in active layers. The 16.71% PCE is achieved in the PM7:Y6:PC₇₁BM (1:1.2:0.2, wt/wt) based OPVs, rooting in the concurrently improved FF of 75.66%, J_{SC} of 25.44 mA cm⁻², and the invariant V_{OC} of 0.868 V. Recently, Yang et al. designed a Y6 derivative named Y6-C2 by moving the branching points of the alkyl chains on the nitrogen atom [97]. The PCE of 15.89% was achieved when blending Y6-C2 with PM6 as active layers. The PC₇₁BM was chosen as the third component due to its good compatibility with Y6-C2. The 17.06% PCE was achieved when the mass ratio of Y6-C2:PC₇₁BM was 1.0:0.2, along with V_{OC} of 0.859 V, J_{SC} of 25.73 mA cm⁻² and FF of 77.2%.

Contrasted with fullerene and non-fullerene-based OPVs, non-fullerene OPVs exhibit more elastic composition modification, providing plenty of chances for improving the performance of OPVs. Absorption spectra, optical bandgap and energy levels of ternary blend films are more widely modulated by two NFAs. Meanwhile, NFAs with similar chemical structures might show good compatibility, which is a considerable element in deciding the phase separation degree and dynamic processes. In this situation, ternary OPVs with two compatible NFAs have attracted much attention in the latest years. In 2019, Zhang et al. reported ternary OPVs based on a newly synthesized NFA 3TP3T-4F and PM6:Y6 system [82]. The compatibility among the materials used was intensively investigated according to a series of characterization methods. According to atomic force microscope (AFM) images, surface morphology and phase separation degree of hybrid films were hardly affected by incorporating 3TP3T-4F as the third component. Measurement of water contact angles (WCAs) for PM6, Y6 and 3TP3T-4F was carried out. The surface tensions (γ) of different materials were 23.3, 25.0 and 25.7 mN m⁻¹ for PM6, Y6 and 3TP3T-4F. The compatibility of two different materials was assessed by applying the equation $\chi \propto (\sqrt{\gamma_A} - \sqrt{\gamma_B})^2$, in which χ represents the Flory–Huggins interaction parameter. The χ parameter between Y6 and 3TP3T-4F is calculated to be 0.0049, indicating excellent compatibility between Y6 and 3TP3T-4F. "To further examine the effect of incorporating 3TP3T-4F on charge separation in active layers, the reorganization energy (λ) was calculated based on the global analysis of the measured Fourier-transform photocurrent spectroscopy, EL spectra and external quantum efficiency (FTPS-EQE), as shown in Figure 9a–e." [82]. The values of λ are 0.066 and 0.081 for PM6:Y6:3TP3T-4F and PM6:Y6 based OPVs, respectively. The slightly reduced reorganization energy at the donor/acceptor interface resulting from incorporation of an appropriate amount of 3TP3T-4F is beneficial to interfacial charge dissociation and transfer in the active layer. PCE of 16.7% is realized when mixing 15 wt% 3TP3T-4F in acceptors, resulting from concurrently increased V_{OC} of 0.85 V, J_{SC} of 25.9 mA cm⁻² and FF of 74.9%. In 2020, Zhang et al. reported ternary OPVs with compatible PM6 as a donor, and MF1 and Y6 as acceptors [38]. "The PCE of 17.22% (certified 16.8%) is realized when mixing 10 wt% MF1 in acceptors, along with V_{OC} of 0.853 V, J_{SC} of 25.68 mA cm⁻² and FF of 78.61%." [38].

It is common knowledge that the V_{OC} s of OPVs mainly are decided by the energy level difference between LUMO of acceptor and HOMO of donor, and energy loss (E_{loss}). In 2019, Zhan et al. proposed a "voltage-increased" approach by employing a second acceptor, which is structurally similar and has a higher LUMO level compared to the host. A PCE of 16.1% is reported by Zhan et al. in PBDB-T-SF:Y6:ITCT based ternary OPVs [98]. The calculated LUMO energy levels of Y6 and ITCT are -4.15 eV and -3.92 eV, respectively. In comparison with Y6, the ITCT:Y6 mixtures with mass ratios of 1:0.5, 1:0.2, and 1:0.1 exhibit higher LUMO energy levels of -4.03, -4.06, and -4.08 eV. V_{OC} s of OPVs

are improved with the increase of ITCT, resulting from uplifted LUMO energy levels by incorporating ITCT. In addition to energy level, the compatibility of the materials used is another consideration for selecting the third component. ITCT and Y6 show homologous structure, which is better for maintaining the film morphology of the host binary. PCE of 16.4% is obtained when the weight ratio of D1/A1/A2 is 1:1.1:0.1, resulting from simultaneously improved V_{OC} of 0.885 V and FF of 73.67%.

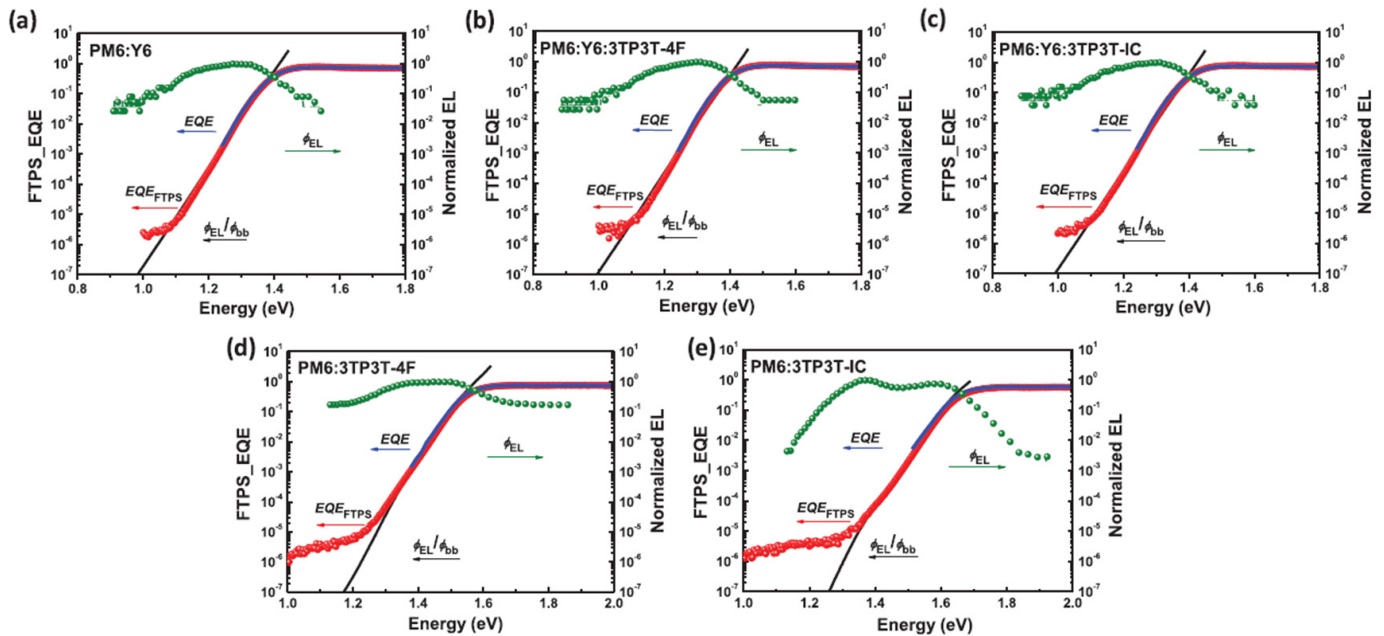


Figure 9. (a–e) Intensity of FTPS-EQE and their fitting. Reproduced from [82]. Reprinted with permission from ref. [82]. Copyright 2019 Wiley.

“The E_{loss} is unavoidable in photoelectric conversion processes involving organic semiconducting materials, which is affected by two key elements. One element is the driving force for charge generation, which is interpreted as the shift between the bandgap of the donor/acceptor materials and the energy of the charge transfer (CT) state.” [99], as shown in Figure 10a. The schematic of two charge-generation pathways in systems with large offset energy is shown in Figure 10b. “The charge can emerge in systems with a large offset energy such that the difference between the lowest singlet exciton energy (S_1 or equivalently E_g) and the charge transfer state (ECT) is greater (case A) or less (case B) than the long-range Coulomb potential (W), which demands to be overcome in order to separate charge and create free carriers beyond their Langevin recombination radius (>5 nm). For low E_{loss} systems, case B will be predominant. Free carriers can be produced from localized CT states either by thermal promotion to delocalized states or by successive hopping.” [99]. A comparatively small driving force takes precedence over realizing rapid and active charge separation. Another element influencing E_{loss} is non-radiative recombination, which can be geminate or non-geminate. The E_{loss} can be divided into three parts based on the Shockley–Queisser (SQ) limit:

$$\begin{aligned}
 E_{loss} &= E_g - eV_{OC} \\
 &= \Delta E_1 + \Delta E_2 + \Delta E_3 \\
 &= (E_g - eV_{OC}^{SQ}) + (eV_{OC}^{SQ} - eV_{OC}^{Rad}) + (eV_{OC}^{Rad} - eV_{OC})
 \end{aligned}$$

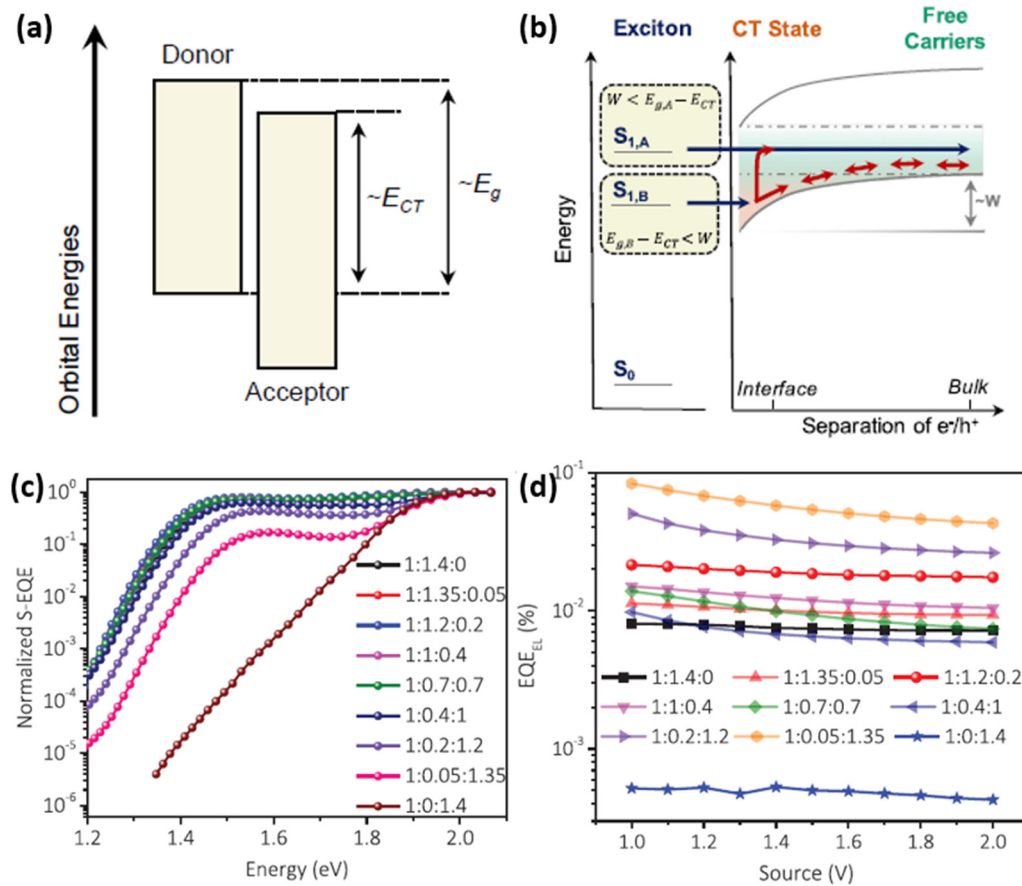


Figure 10. (a) Diagram of organic solar cell orbital energetics for a typical donor-acceptor pairing. (b) Schematic of two charge-generation pathways in systems with a large offset energy. Reproduced from [99]. (c) Normalized s-EQEs and (d) EQE_{EL} values of the binary and ternary devices. Reproduced from [100].

“In this formula, ΔE_1 means inevitable radiative recombination loss above the bandgap, which represents the difference between E_g and maximum voltage V_{OC}^{SQ} based on the SQ limit.” [39]. ΔE_2 represents radiative recombination loss below the bandgap, and V_{OC}^{Rad} is the voltage when premeditating the actual radiative recombination. ΔE_3 means non-radiative loss, which is linearly bound with the natural logarithm of EQE_{EL} , as represented by $\Delta E_3 = -KT \ln(EQE_{EL})$. Minimizing E_{loss} with ternary strategy is now an emergent channel for achieving performance improvement of OPVs. In 2019, Hou et al. reported the reduced E_{loss} of ternary OPVs by mixing fullerene-derived PC₆₁BM as the third component into the PM6:Y6 system [100]. PCE of 16.5% is realized in the optimized ternary OPVs, along with V_{OC} of 0.845 V, J_{SC} of 25.4 mA cm⁻², and FF of 77%. The optimized ternary OPVs with a mass ratio of PM6:Y6:PC₆₁BM of 1:1.2:0.2 showed the largest EQE_{EL} of 1.9×10^{-4} , as shown in Figure 10c,d. The calculated ΔE_3 is 0.25 eV, 0.22 eV and 0.32 eV for the PM6:Y6, optimized ternary and PM6:PC₆₁BM devices, respectively, indicating the reduced non-radiative recombination by employing ternary strategy. In 2020, Zhang et al. reported ternary OPVs with PM6:BTP-4F-12:MeIC as the active layer [39]. A PCE of 17.4% is realized when mixing 15 wt% MeIC in acceptors, resulting from FF of 79.2%, V_{OC} of 0.863 V and J_{SC} of 25.4 mA cm⁻². “Photon harvesting, exciton dissociation and charge transport of ternary active layers can be synergistically improved by mixing 10 wt% MeIC in acceptors.” [39]. At the same time, the minimized E_{loss} of 0.526 eV can be realized in the PM6:BTP-4F-12:MeIC(1:1.08:0.12, wt/wt) based OPVs, leading to enhanced V_{OC} of ternary OPVs. The detailed E_{loss} of blend OPVs was further studied by EQE_{EL} spectra and highly sensitive EQE (s-EQE) spectra. The addition of MeIC did not bring about any extra absorption or emission of subgap states, causing ΔE_2 of ternary OPVs to approach

the BTP-4F-12 based ternary OPVs. The ternary OPVs exhibit an EQE_{EL} of 1.58×10^{-4} , which is higher than those of two binary OPVs, resulting in reduced non-radiative loss of 0.227 eV. Reduced non-radiative loss might cause performance improvement of PM6:BTP-4F-12:MeIC(1:1.08:0.12, wt/wt) based OPVs.

In comparison with the polymer/small molecule blend systems, all-polymer based OPVs consisting of tightly entangled polymer acceptor and donor, tend to possess better operational lifetime due to their outstanding morphological and device stabilities under mechanical and thermal stresses. In 2021, Min et al. designed a near-infrared polymer acceptor (P_A) PY2F-T, and the all-polymer solar cells (all-PSCs) achieved a 15.0% PCE by blending PM6 as the donor [37]. Subsequently, PYT was incorporated into the PM6: PY2F-T main system as the third component. The PM6:PY2F-T:PYT based all-PSCs achieved V_{OC} of 0.90 V, J_{SC} of 25.2 mA cm^{-2} , FF of 76% and a high PCE of 17.2% (certified PCE of 16.9%). Contrasted with the PM6:PY2F-T system, the ternary OPVs exhibits lower energy loss, better light absorption and light thermal stability. This work promotes the development of high-performance ternary all-PSCs and creates possibilities for their application.

3.1.3. Typical Works on Quaternary OPVs

Ternary strategy has been proved to be an efficient means to improve the performance of OPVs by mixing a donor or acceptor into the host binary system. Building on the foundation of ternary OPVs and to pursue highly efficient OPVs, more attempts such as quaternary strategy emerged for utilizing multicomponents with a complementary absorption spectrum. The third and fourth components can work independently to optimize performance of OPVs step-by-step, which further explores the potential of materials. In general, photon harvesting, photogenerated exciton distribution, exciton dissociation and charge transport in quaternary active layers can be individually or simultaneously improved by successively mixing the desirable third or fourth component. It should be noted that the dynamic process of excitons and charge carriers is exceptionally complicated, involving four functional components in active layers, which makes the selection of appropriate active layer materials very challenging. Before 2019, quaternary OPVs with more than 14% PCE had never been realized, which was far behind the development of ternary OPVs. Generally, a quaternary OPV is composed of two fullerene derivatives and one NFA. Actually, choosing fullerene derivatives as the third and fourth components in quaternary OPV may not be an ideal strategy. The fullerene derivatives may be the outstanding fourth component based on favorable ternary non-fullerene OPVs.

Benefiting from the rapid development of highly efficient active materials, over 16% PCE is realized in quaternary OPVs. In 2020, Zhang et al. reported highly efficient quaternary OPVs with PM6:Y6:Br-ITIC:PC₇₁BM as the active layer [101]. "A PCE of 15.7% is realized in the PM6:Y6 based binary OPVs, along with V_{OC} of 0.841 V, J_{SC} of 25.2 mA cm^{-2} , and FF of 74.3%. The PCEs of 16.4% and 16.2% can be achieved by mixing a suitable amount of PC₇₁BM and Br-ITIC as the third component, respectively, corresponding to the J_{SC} of 25.6 vs. 25.5 mA cm^{-2} , V_{OC} of 0.836 vs. 0.854 V and FF of 75.6% vs. 75.1%." [101]. Based on optimized ternary OPVs, PC₇₁BM is mixed as a morphology regulator to commendably improve phase separation and molecular arrangement of the active layer of the mixed film, resulting in an improved PCE of 16.8% with further marginally increased FF of 76.4% and J_{SC} of 25.8 mA cm^{-2} . The drop of EQE spectrum for the PM6:Y6 based binary OPV in the wavelength range of 650 to 800 nm can be gradually compensated by continuously adding suitable amounts of Br-ITIC and PC₇₁BM, which can be clearly observed from the amplified EQE spectrum. The optimized phase separation in the quaternary active layer improves exciton dissociation and charge transport, resulting in enhanced EQE values in the long wavelength range. "The optical field distribution in OPVs and photogenerated exciton density in active layers were simulated by using the transfer matrix method" [101], as shown in Figure 11a–f. The calculated values of photogenerated exciton density are 3.52×10^{29} , 3.47×10^{29} and $3.46 \times 10^{29} \text{ s}^{-1} \text{ m}^{-3}$ in the quaternary, ternary and binary blend films, which supports the J_{SC} improvement of ternary OPVs. "The hole and electron

produced in the middle region are likely to be simultaneously collected by the electrode because of their similar transport distance. Here, the calculated photogenerated exciton density values in the middle 50 nm region of active layer are 2.22×10^{29} , 2.20×10^{29} and $2.18 \times 10^{29} \text{ s}^{-1} \text{ m}^{-3}$ in the optimized quaternary, ternary and binary active layers." [101]. Enhanced photogenerated exciton density in the near-middle region of the ternary active layers should be beneficial to balance charge collection and transport. According to the space-charge limited-current (SCLC) method, the charge transport property was further investigated. The μ_h/μ_e ratio decreased from 5.0 to 1.9 and 1.2 by successively incorporating Br-ITIC and PC₇₁BM. By mixing suitable Br-ITIC and PC₇₁BM into blend films, a gradually balanced charge transfer was realized, which is conducive to the gradual improvement of FF.

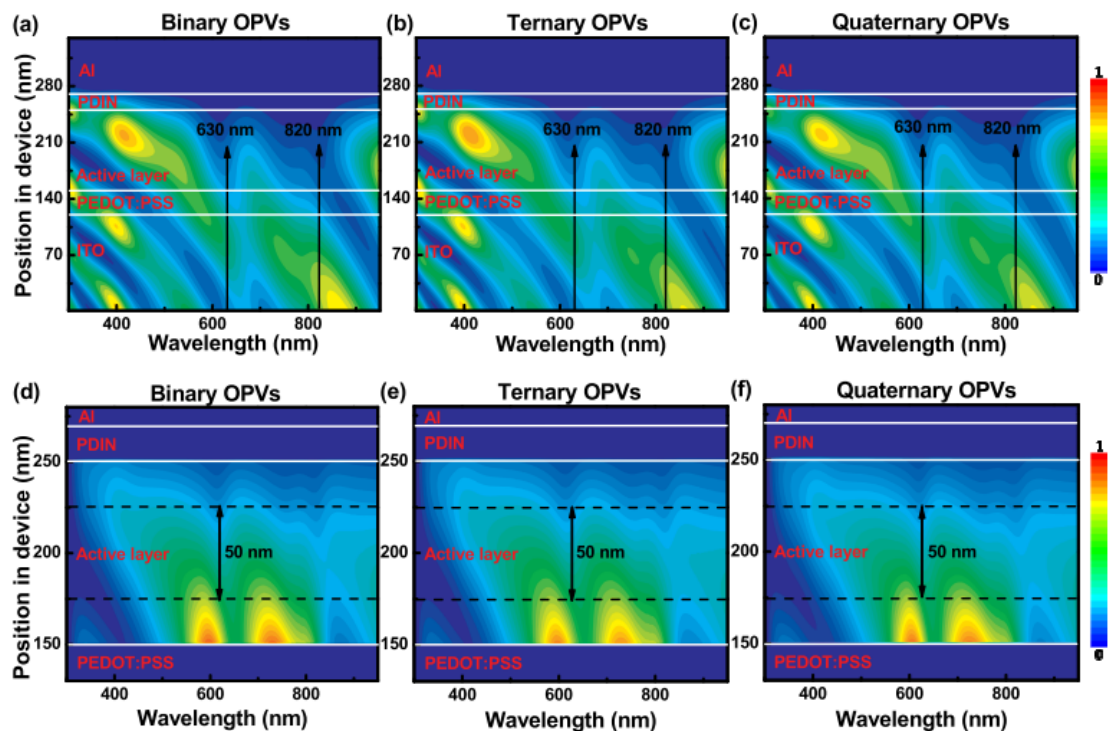


Figure 11. The simulated optical field distribution in the (a) binary, (b) ternary and (c) quaternary OPVs; calculated photogenerated exciton distribution in the optimized active layers of (d) binary, (e) ternary and (f) quaternary OPVs. Reproduced from [101]. Reprinted with permission from ref. [101]. Copyright 2020 Elsevier.

In the same year, another efficient quaternary OPV was reported by Zhan et al., developed by incorporating a newly synthesized polymer donor material PhI-Se and commonly used fullerene derivative PC₇₁BM into an efficient binary system PM6:Y6 [51]. Solid-state ¹⁹F magic angle spinning nuclear magnetic microscopy (¹⁹F MAS NMR), GIWAXS, elemental TEM mapping and transient absorption spectroscopy on corresponding films were carried out to investigate molecular structures and charge separation dynamic processes in active layers. In this quaternary system, Se is selectively decorated on PhI-Se, N is seen on PhI-Se and Y6, and F is modified on PM6 and Y6. Overlapping plots of the N and Se, F and Se, and N + F + Se mapping data (Figure 12) indicate that the incorporated PhI-Se prefer to form individual PhI-Se phases, which are interpenetrating with the PM6 and Y6 phases. The individual PhI-Se phase can enhance solar light absorption and function as additional paths for charge separation and hole transport. According to ¹⁹F MAS NMR spectroscopy and GIWAXS characterization results, the long-ranged structural order of acceptor phases can be improved by incorporating PhI-Se, which is beneficial to electron transport. A maximum PCE of 17.2% can be achieved in quaternary OPVs with the weight ratios of PhI-Se:PM6:Y6:PC₇₁BM as 0.15:1:1.2:0.20. Recently, a 17.73% PCE of quaternary OPVs was

reported by Zhang et al. by using two polymer donors (PM6 and PTQ10) and two acceptors (N3 and PC₇₁BM) as the active layer [53]. The small domains of PTQ10 and PC₇₁BM play the role of separators to spatially separate PM6 and N3, forming a “rivers-and-streams”-like morphology. The hierarchical morphology can create respective pathways for both holes and electrons to transport across the active layer with suppressed recombination losses. Currently, the occurrence of highly efficient quaternary OPVs suggests that the development of quaternary OPVs can be gradually compared with that of binary and ternary OPVs. With careful material selection and morphology control, quaternary strategy can also play a key role in performance improvement of OPVs.

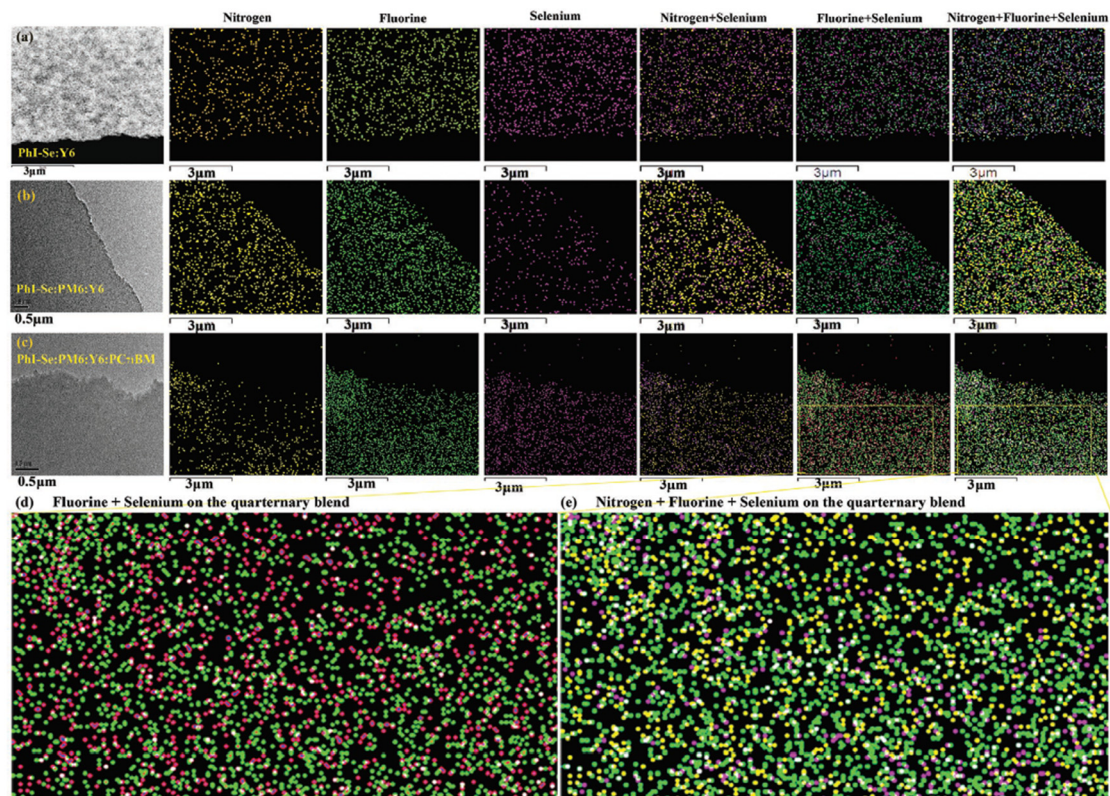


Figure 12. (a–c) Distribution of N, F and Se; (d,e) enlarged pictures. Reproduced from [51]. Reprinted with permission from ref. [51]. Copyright 2020 Wiley.

3.2. Tandem Structure OPVs

Based on the Shockley–Queisser (SQ) assumptions, there are two main losses in single junction OPVs: thermalization loss due to photons of higher energy than the bandgap and transmission loss resulting from low energy photons beyond the organic semiconducting material optical band edge [102,103]. An effective strategy to overcome the SQ limits is to construct tandem OPVs. Tandem OPVs are, in general, made of different bandgap materials to prepare double or multiple active layers connected by the middle electrode. Based on the connection methods of the subcells, the tandem OPVs can be divided into two categories: series and parallel tandem structures. The series tandem OPVs are designed to exhibit increased V_{OC} values, which correspond to the sum of the V_{OC} values for each subcell. The parallel tandem OPVs are prepared in order to obtain enhanced J_{SC} , which is equivalent to the sum of the J_{SC} of each subcell.

Tandem strategy has emerged as an active means to achieve the performance improvement of OPVs. A series of successful works have been completed by many research groups. Especially, in 2018, Chen et al. reported a record and certified PCE of 17.29% for 2-terminal (2T) monolithic solution-processed tandem OPVs [104]. The semi-empirical analysis was carried out by Chen et al. for the possible PCE limit of 2T tandem OPV cells

under AM 1.5G illumination. Based on the model analysis, CO₂8DFIC was selected as the acceptor of the rear subcell due to its infrared absorption onset of ~1050 nm (optical bandgap E_g 1.20 eV). The PTB7-Th:CO₂8DFIC:PC₇₁BM based single junction OPVs exhibit a high J_{SC} of 27.98 mA cm⁻², FF of 69.7%, V_{OC} of 0.69 V and rather low E_{loss} of 0.51 eV. The PBDB-T and F-M were selected as the donor and acceptor of the active layer of the front cell, which led to the absorption onset of the active layer mixture approaching 720 nm. The PBDB-T:F-M based single junction OPVs show V_{OC} of 0.94 V, J_{SC} of 15.96 mA cm⁻², and FF of 69.8%. It is known that the high and balanced J_{SC} is one of the preconditions for fabricating efficient 2T tandem OPVs. A remarkable PCE of 17.36% (certified 17.29%) can be achieved in the optimized 2T tandem OPVs, with J_{SC} of 14.35 mA cm⁻², V_{OC} of 1.642 V and FF of 73.7%.

Except for the selection of complementary active layer materials for harvesting more photons, the middle layer between two or more subcells is another key component for constructing efficient tandem OPVs. The middle layer (also called interconnecting layer) is a combination of an ultrathin hole extraction layer and electron extraction layer. An ideal middle layer should pass light and sustain the photocurrent by providing an optically transparent electrical contact for recombination of holes and electrons from the adjacent active layers [105]. In addition, the middle layer should provide chemical protection for the front subcell against dissolution from the solution processing of the back. These requirements severely limit the selection of the middle layer, which makes it challenging for fabricating highly efficient and reproducible tandem OPVs. In 2020, a simple and highly compatible middle layer of PEDOT:PSS HTL (HSolar)/ZnO in an inverted tandem OPVs was reported by So et al. [106]. Compared to the traditional PEDOT:PSS Al 4083 (c-PEDOT), the HSolar possesses a superior wettability on the underlying non-fullerene active layer, leading to superior charge carrier extraction features of the middle layer. The tandem OPVs were fabricated by employing FTAZ:IT-M as the front cell and PTB7-Th:IEICO-4F as the back cell. The optimized tandem OPVs present PCE of 14.7%, with V_{OC} of 1.65 V, J_{SC} of 14.6 mA cm⁻² and FF of 61%. To demonstrate the generality of the middle layer process, the middle layer process recipe was shared with other research groups. All of the double-junction tandem OPVs based on distinct active layers exhibited high repeatability in several different laboratories without a significant loss in V_{OC} and FF. Among these tandem OPVs, the highest 16.1% PCE was achieved by using the front cell based on PBDB-T:F-M and the back cell based on PTB7-Th:IEICO-4F. To further demonstrate the versatility of the HSolar process, homo triple-junction OPVs were prepared using PTB7-Th:IEICO-4F as the active layer. Device architecture was ITO/ZnO/active layer/HSolar/ZnO/active layer/HSolar/ZnO/active layer/MoOx/Ag. Based on the transfer matrix model simulation, the optimum thickness of the front, middle and back cell should be approximately 50, 90, and 120 nm, respectively. The PCE of optimized homo triple-junction OPVs reached 11.2%, which is higher than 9.9% in the corresponding single junction OPVs. In 2021, Huang et al. developed an effective interconnect layer based on the structure of ZnO NPs: PEI/PEI/PEDOT: PSS [107]. The optimal thickness of the pre-cell in these tandem OPVs was reduced by increasing the proportion of NFAs in the active layers to inhibit charge recombination. Tandem OPVs were designed based on the structure ITO/PEDOT:PSS/front cell/ZnO NPs:PEI/PEI/PEDOT:PSS/back cell/PNDIT-F3N/Ag. The front cell was PM7:TfIF-4Cl, and the back cell was PCE10:CO₂8DFIC:PC₇₀BM. Finally, the optimal PCE was 18.71% (certified by an accredited institute to be 18.09%) with J_{SC} of 14.59 mA cm⁻², V_{OC} of 1.64 V and FF of 78%. The various syntheses of highly efficient NFAs together with matched polymer donors brings more opportunity for further development of tandem OPVs. So et al. simulated a tandem OPVs by employing FTAZ:IT-M and PM6:Y6 as front cell and back cell, respectively, predicting the possibility of tandem OPVs with a PCE over 22%.

It is undeniable that tandem strategy shows great potential for further improving OPVs and pushing PCE to a new level. It should be also noted that the relatively complicated fabrication process of tandem OPVs still limits their future commercial application.

Currently, another emerging tandem solar cell, IPOSCs, has recently attracted attention due to its simplified fabrication process. IPOSCs are constructed by employing a wide bandgap perovskite-based front cell and narrow bandgap organic-material-based rear cell. The organic materials can be dissolved in orthogonal solvents and then deposited on the perovskite layer without the existence of a recombination layer. Recent rapid development of narrow bandgap organic semiconductors provides various excellent candidates as the back cells. In 2019, He et al. used a polymer donor S1, an NFA Y6, together with PCBM to form a ternary BHJ layer [108]. The ternary organic BHJ layers were then integrated into the top layer of the perovskite to extend the NIR photo response up to 980 nm. Finally, a record J_{SC} (28.06 mA cm^{-2}) for perovskite solar cells with a 1.6 eV bandgap material was achieved based on single-junction structure. This result demonstrates that the IPOSCs have a huge potential to break the single-junction SQ efficiency limits.

3.3. Interface Engineering in OPVs

In addition to the development of donors or acceptors, interface engineering is also crucial for the preparation of high efficiency OPVs. In 2020, Zhang et al. developed an aliphatic amine group, functionalized PDI derivative (PDINN) as a cathode interlayer material (CIM) in the OPVs, and used stable metals (silver and copper) in the air as the top cathode [25]. Due to the presence of the aliphatic amine group, PDINN has a suitable dipole moment, thereby reducing the work function (WF) of air-stable metals (silver and copper). The hydrogen bonds can be formed between the secondary amine in the PDINN side chain and photovoltaic materials, leading to an excellent connection with the active layer. As compared to generally employed CIM PDINO, the PDINN has relatively good contact with NFA based active layers, relatively strong capacity to decrease metal cathode WFs, relatively high electrical conductivity ($5.0 \times 10^{-4} \text{ S cm}^{-1}$) and stronger charge collection ability. At the same time, OPVs based on PDINN show excellent tolerance to the variation of PDINN thickness when manufacturing devices. For example, when the PDINN thickness is expanded to 27 nm, PCE of the devices remains above 15.0%. What is impressive is that when the thickness of PDINN is increased to 38 nm, FF remains at 74.09%, which is very important for large-area manufacturing of OPVs. In addition, PDINN also has the advantages of easy synthesis and low cost in the laboratory. PM6:Y6 was employed as the active layer to prepare all OPVs. Finally, the PCE of the PDINO/Ag based device is 15.17%, the V_{OC} is 0.821 V, J_{SC} is 25.58 mA cm^{-2} , and FF is 72.24%. The maximum PCE of devices with the PDINN/Ag cathode is even higher, reaching 17.23%. Compared with PDINO/Ag based devices, the significant increased efficiency in PDINN/Ag based devices is due to the substantial improvement in photovoltaic parameters: V_{OC} increased from 0.821 to 0.847 V and FF increased from 72.24% to 78.59%. This result suggests that regulating interfacial contact with proper intermolecular interactions should be a feasible method to enhance the performance of thin-film OPVs.

PEDOT:PSS is a popular anode interface material because of its good film forming property and excellent optical transparency [109]. In 2020, Huang et al. introduced dopamine hydrochloride (DA·HCl) into PEDOT:PSS, considering that there are excess sulfonic acid groups in the PSS of PEDOT:PSS [110]. The ion exchange reaction between PSS and DA·HCl produces PSS-DA. The PSS-DA segment has stronger intermolecular accumulation in PEDOT:PSS-DA, thus improving the aggregation of the PEDOT main chain and the electronic conductivity of PEDOT:PSS. Finally, by employing PEDOT:PSS-DA as an anode interface material instead of PEDOT:PSS, the PCEs of PM6:Y6, PBDB-T:ITIC and PM6:IDIC, and P3HT:PC61BM based OPVs were concurrently increased. The results show that incorporating amino derivatives into PEDOT:PSS is an effective method to improve the performance of OPVs.

In 2019, Anthopoulos et al. used liquid-exfoliated 2D transition metal disulfides (WS_2 and MoS_2 nanosheets) as HTLs directly coated on transparent ITO electrodes to change WF without further treatment [33]. Initially, WS_2 and MoS_2 were exfoliated by using previously reported protocols, as shown in Figure 13a. Figure 13b presents absorption spectra of the

extracted WS₂ and MoS₂ flakes in ethanol:water. “As-prepared MX₂ suspensions were spin-coated onto ITO without any further treatment (Figure 13c).” [33]. Subsequently, to investigate surface morphology of the ITO, AFM images were characterized as shown in Figure 13d. Among these two MX₂ systems, ITO/WS₂ exhibited the smoothest surface topography. WS₂ flakes became larger and thinner compared to MoS₂. By combining WS₂ HTLs with PBDB-T-2F:Y6 and PBDB-T-2F:Y6:PC₇₁BM BHJ systems, the greatest PCE of 15.8% and 17% OPVs can be achieved, respectively. After investigation, the good photonic structure and restrained recombination loss of WS₂ based OPVs resulted in higher efficiency.

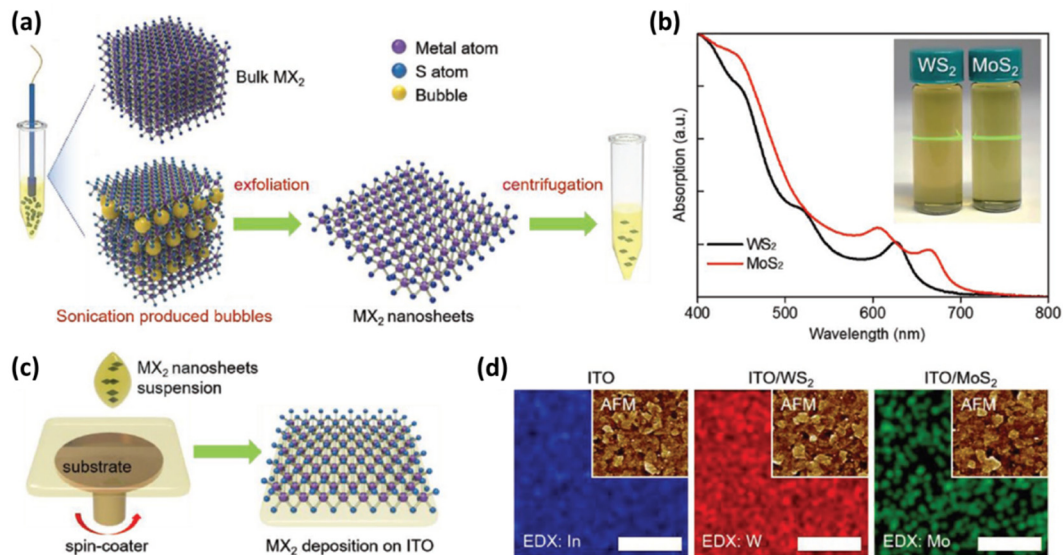


Figure 13. (a) The preparation process of MoS₂ and WS₂ suspensions. (b) Absorption spectra and the Tyndall effect in WS₂ and MoS₂ dispersions. (c) Schematic diagram of deposition of MoS₂ and WS₂ HTLs on substrate. (d) Element mapping obtained using EDX (scale bar: 2 μm). Insets exhibit AFM images of corresponding samples. Reproduced from [33]. Reprinted with permission from ref. [33]. Copyright 2019 Wiley.

Polyoxometalate-based inorganic clusters (PICs) have the characteristics of easy preparation and purification of organic molecules and high WF of metal oxides. However, due to the limitation of quantum tunneling effect, the PIC film’s hole transport ability is usually poor. In 2021, Hou et al. significantly enhanced the PICs’ conductivity ($2.6 \times 10^{-3} \text{ S m}^{-1}$) on the basis of molybdenum and oxygen without influencing their relatively high WF property by mixing HPMO with bivalent tin (17:3) in methanol [111]. The chemical structure of HPMO is presented in Figure 14a. By employing HPMO as the HTL, the PM6:BTP-eC9 based OPVs presented a very low 0.25% PCE. “However, the device based on the HPMO:Sn (17:3) blend exhibited a high 17.3% PCE, along with V_{OC} of 0.84 V, J_{SC} of 26.8 mA cm^{-2} , and FF of 77%, which were comparable to the best results for the PEDOT:PSS device.” [111]. The J - V curves and EQE spectra of corresponding devices are shown in Figure 14b,c. In order to study the HPMO:Sn’s universality, PTB7-Th:PC₇₁BM, PBDB-T:ITIC and PM6:IT-4F were selected as the active layer to manufacture OPVs. Finally, the three OPVs’ PCEs were comparable with their original PCEs reported in the literature, which indicates that HPMO:Sn can be generally used as HTL material. Furthermore, a 1.0 cm^2 device (HPMO:Sn as HTL) made by the blade-coated method displayed a 15.1% PCE (Figure 14d), which was the record-breaking value for large-area OPVs. Figure 14d also presents the EQE mapping image, which indicates that about 80% of EQE is achieved. This result shows that HPMO:Sn is a high-performance HTL, which is low-cost, easy to prepare and compatible with a large-area printing process.

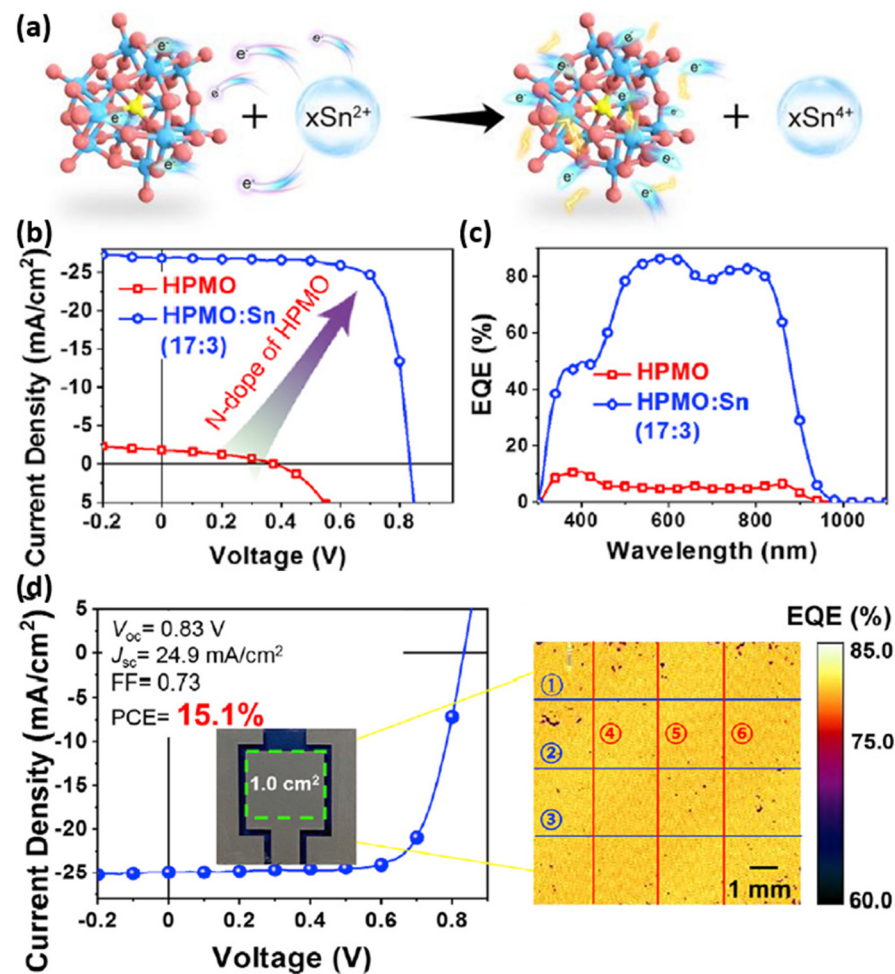


Figure 14. (a) Diagram of the reaction. (b) J - V curves and (c) EQE spectra of corresponding OPVs. (d) J - V curves and photovoltaic parameters of 1 cm^2 OPVs. Mapping image of EQE at 500 nm. Reproduced from [111]. Reprinted with permission from ref. [111]. Copyright 2021 Elsevier.

In the field of hybrid perovskite solar cells, self-assembled monolayers (SAMs) of organic small molecules have recently been developed to replace commonly used HTL materials, thereby enhancing PCE and improving stability of the cells. Surprisingly, the application of a SAM interlayer in OPVs has only attracted limited attention, so far. In 2021, Anthopoulos et al. reported that Br-2PACz modified ITO was used as a hole-extracting interlayer in OPVs based on PM6:BTP-eC9:PC₇₁BM. The maximum PCE of OPVs reached 18.4%, which was higher than the PCE value based on PEDOT:PSS (17.5%) [112]. It is found that the relatively high PCE is due to the relatively high WF (-5.81 eV) of ITO/Br-2PACz as compared to ITO/PEDOT:PSS (4.9 eV), and the better active layer morphology with Br-2PACz as HTL. The synergistic effects induced by Br-2PACz SAM result in cells with lower interface resistance, increased hole mobility and longer carrier lifetime. The important aspect is that the ITO/Br-2PACz electrode is chemically stable. The SAM removed can be recycled and reused to build OPVs with the same excellent performance. Therefore, Br-2PACz has the characteristics of process ability, low cost, adjustable electronic properties and chemical stability, which means that OPVs can be prepared with high efficiency and high stability.

4. Summary and Perspectives

Over 18% PCE has been realized in single active layer and tandem structure OPVs in recent years, benefiting from the development of novel donor and acceptor materials, modification materials of the interface layer and device engineering. With the significant

improvement of OPV equipment performance, the next step will be to make the technology more suitable for scale-up and commercialization. A list of possible future research directions follows: (1) At present, NFAs and wide bandgap donors have great development potential. Optimizing the structure of existing high-performance materials or developing novel materials with high charge mobility and low energy loss will play a vital role in constructing thick-film-based OPVs for meeting future commercial production. In-depth photophysical mechanism research of highly efficient OPV is also required, which can afford more valuable suggestions for material synthesis with higher performance. (2) Ternary OPV can achieve a wide absorption spectrum in a single active layer; tandem OPV can break through the Shockley–Queisser limit of single junction devices and achieve high V_{OC} . The combination of ternary strategy and tandem devices may be a promising method that can visibly increase PCE by more than 20%. (3) A good interface modification layer is also crucial for the commercialization of OPV. The future development direction of interface modification layer materials might be excellent performance, simple preparation process, low cost and good compatibility with a large area printing process. (4) At the same time, exploring halogen-free and environment friendly green solvents and promoting the use of non-toxic solvent printing technology would all be conducive to environmental protection.

Author Contributions: Conceptualization, Q.S., J.G. and C.X.; writing—original draft preparation, X.W. and X.M.; writing—review and editing, X.M., J.W. and F.Z.; supervision, F.Z. All authors have read and agreed to the published version of the manuscript.

Funding: This research received no external funding.

Acknowledgments: This work was supported by the National Natural Science Foundation of China (61975006, 62075155), Postdoctoral Innovative Talent Support Program (BX20200042), China Postdoctoral Science Foundation (2020M680327), Beijing Natural Science Foundation (4192049).

Conflicts of Interest: The authors declare no conflict of interest.

References

1. Zhang, Y.; Wang, J.; Wang, X. Review on probabilistic forecasting of wind power generation. *Renew. Sustain. Energy Rev.* **2014**, *32*, 255–270. [[CrossRef](#)]
2. Lewis, N.S. Toward Cost-Effective Solar Energy Use. *Science* **2007**, *315*, 798–801. [[CrossRef](#)] [[PubMed](#)]
3. De Arquer, F.P.G.; Armin, A.; Meredith, P.; Sargent, E.H. Solution-processed semiconductors for next-generation photodetectors. *Nat. Rev. Mater.* **2017**, *2*, 16100. [[CrossRef](#)]
4. Gao, W.; An, Q.; Hao, M.; Sun, R.; Yuan, J.; Zhang, F.; Ma, W.; Min, J.; Yang, C. Thick-Film Organic Solar Cells Achieving over 11% Efficiency and Nearly 70% Fill Factor at Thickness over 400 nm. *Adv. Funct. Mater.* **2020**, *30*, 1908336. [[CrossRef](#)]
5. An, Q.; Wang, J.; Zhang, F. Ternary polymer solar cells with alloyed donor achieving 14.13% efficiency and 78.4% fill factor. *Nano Energy* **2019**, *60*, 768–774. [[CrossRef](#)]
6. Wu, J.-S.; Cheng, S.-W.; Cheng, Y.-J.; Hsu, C.-S. Donor–acceptor conjugated polymers based on multifused ladder-type arenes for organic solar cells. *Chem. Soc. Rev.* **2015**, *44*, 1113–1154. [[CrossRef](#)]
7. Hu, Z.; Wang, Z.; An, Q.; Zhang, F. Semitransparent polymer solar cells with 12.37% efficiency and 18.6% average visible transmittance. *Sci. Bull.* **2020**, *65*, 131–137. [[CrossRef](#)]
8. Kwon, O.K.; Uddin, M.A.; Park, J.-H.; Park, S.K.; Nguyen, T.L.; Woo, H.Y.; Park, S.Y. A High Efficiency Nonfullerene Organic Solar Cell with Optimized Crystalline Organizations. *Adv. Mater.* **2016**, *28*, 910–916. [[CrossRef](#)]
9. Ma, X.; Zhang, F.; An, Q.; Sun, Q.; Zhang, M.; Zhang, J. Dramatically Boosted Efficiency of Small Molecule Solar Cells by Synergistically Optimizing Molecular Aggregation and Crystallinity. *ACS Sustain. Chem. Eng.* **2017**, *5*, 1982–1989. [[CrossRef](#)]
10. Zomeran, D.; Kong, J.; McAfee, S.M.; Welch, G.C.; Kelly, T.L. Control and Characterization of Organic Solar Cell Morphology Through Variable-Pressure Solvent Vapor Annealing. *ACS Appl. Energy Mater.* **2018**, *1*, 5663–5674. [[CrossRef](#)]
11. An, Q.; Ma, X.; Gao, J.; Zhang, F. Solvent additive-free ternary polymer solar cells with 16.27% efficiency. *Sci. Bull.* **2019**, *64*, 504–506. [[CrossRef](#)]
12. Schilinsky, P.; Waldauf, C.; Brabec, C.J. Recombination and loss analysis in polythiophene based bulk heterojunction photodetectors. *Appl. Phys. Lett.* **2002**, *81*, 3885–3887. [[CrossRef](#)]
13. Gao, J.; Wang, J.; Xu, C.; Hu, Z.; Ma, X.; Zhang, X.; Niu, L.; Zhang, J.; Zhang, F. A Critical Review on Efficient Thick-Film Organic Solar Cells. *Sol. RRL* **2020**, *4*, 2000364. [[CrossRef](#)]
14. Zeng, A.; Ma, X.; Pan, M.; Chen, Y.; Ma, R.; Zhao, H.; Zhang, J.; Kim, H.K.; Shang, A.; Luo, S.; et al. A Chlorinated Donor Polymer Achieving High-Performance Organic Solar Cells with a Wide Range of Polymer Molecular Weight. *Adv. Funct. Mater.* **2021**, *31*, 2102413. [[CrossRef](#)]

15. Hu, Z.; Wang, J.; Wang, Z.; Gao, W.; An, Q.; Zhang, M.; Ma, X.; Wang, J.; Miao, J.; Yang, C.; et al. Semitransparent ternary nonfullerene polymer solar cells exhibiting 9.40% efficiency and 24.6% average visible transmittance. *Nano Energy* **2019**, *55*, 424–432. [[CrossRef](#)]
16. Lin, Y.; Wang, J.; Zhang, Z.-G.; Bai, H.; Li, Y.; Zhu, D.; Zhan, X. An Electron Acceptor Challenging Fullerenes for Efficient Polymer Solar Cells. *Adv. Mater.* **2015**, *27*, 1170–1174. [[CrossRef](#)]
17. Zhao, W.; Qian, D.; Zhang, S.; Li, S.; Inganäs, O.; Gao, F.; Hou, J. Fullerene-Free Polymer Solar Cells with over 11% Efficiency and Excellent Thermal Stability. *Adv. Mater.* **2016**, *28*, 4734–4739. [[CrossRef](#)] [[PubMed](#)]
18. Zhao, Z.; Xu, C.; Niu, L.; Zhang, X.; Zhang, F. Recent Progress on Broadband Organic Photodetectors and their Applications. *Laser Photon. Rev.* **2020**, *14*, 2000262. [[CrossRef](#)]
19. Yuan, J.; Zhang, Y.; Zhou, L.; Zhang, G.; Yip, H.-L.; Lau, T.-K.; Lu, X.; Zhu, C.; Peng, H.; Johnson, P.A.; et al. Single-Junction Organic Solar Cell with over 15% Efficiency Using Fused-Ring Acceptor with Electron-Deficient Core. *Joule* **2019**, *3*, 1140–1151. [[CrossRef](#)]
20. Luo, Z.; Ma, R.; Liu, T.; Yu, J.; Xiao, Y.; Sun, R.; Xie, G.; Yuan, J.; Chen, Y.; Chen, K.; et al. Fine-Tuning Energy Levels via Asymmetric End Groups Enables Polymer Solar Cells with Efficiencies over 17%. *Joule* **2020**, *4*, 1236–1247. [[CrossRef](#)]
21. Cui, Y.; Yao, H.; Zhang, J.; Xian, K.; Zhang, T.; Hong, L.; Wang, Y.; Xu, Y.; Ma, K.; An, C.; et al. Single-Junction Organic Photovoltaic Cells with Approaching 18% Efficiency. *Adv. Mater.* **2020**, *32*, 1908205. [[CrossRef](#)] [[PubMed](#)]
22. Ma, Y.; Zhang, M.; Wan, S.; Yin, P.; Wang, P.; Cai, D.; Liu, F.; Zheng, Q. Efficient Organic Solar Cells from Molecular Orientation Control of M-Series Acceptors. *Joule* **2021**, *5*, 197–209. [[CrossRef](#)]
23. Cui, Y.; Yao, H.; Hong, L.; Zhang, T.; Tang, Y.; Lin, B.; Xian, K.; Gao, B.; An, C.; Bi, P.; et al. 17% efficiency organic photovoltaic cell with superior processability. *Natl. Sci. Rev.* **2019**, *7*, 1239–1246. [[CrossRef](#)]
24. Ma, R.; Liu, T.; Luo, Z.; Guo, Q.; Xiao, Y.; Chen, Y.; Li, X.; Luo, S.; Lu, X.; Zhang, M.; et al. Improving open-circuit voltage by a chlorinated polymer donor endows binary organic solar cells efficiencies over 17%. *Sci. China Chem.* **2020**, *63*, 325–330. [[CrossRef](#)]
25. Yao, J.; Qiu, B.; Zhang, Z.-G.; Xue, L.; Wang, R.; Zhang, C.; Chen, S.; Zhou, Q.; Sun, C.; Yang, C.; et al. Cathode engineering with perylene-diimide interlayer enabling over 17% efficiency single-junction organic solar cells. *Nat. Commun.* **2020**, *11*, 2726. [[CrossRef](#)]
26. Wang, T.; Sun, R.; Shi, M.; Pan, F.; Hu, Z.; Huang, F.; Li, Y.; Min, J. Solution-Processed Polymer Solar Cells with over 17% Efficiency Enabled by an Iridium Complexation Approach. *Adv. Energy Mater.* **2020**, *10*, 2000590. [[CrossRef](#)]
27. Wu, J.; Li, G.; Fang, J.; Guo, X.; Zhu, L.; Guo, B.; Wang, Y.; Zhang, G.; Arunagiri, L.; Liu, F.; et al. Random terpolymer based on thiophene-thiazolothiazole unit enabling efficient non-fullerene organic solar cells. *Nat. Commun.* **2020**, *11*, 4612. [[CrossRef](#)]
28. Zhu, C.; Meng, L.; Zhang, J.; Qin, S.; Lai, W.; Qiu, B.; Yuan, J.; Wan, Y.; Huang, W.; Li, Y. A Quinoxaline-Based D–A Copolymer Donor Achieving 17.62% Efficiency of Organic Solar Cells. *Adv. Mater.* **2021**, *33*, 2100474. [[CrossRef](#)] [[PubMed](#)]
29. Zhang, Z.; Li, Y.; Cai, G.; Zhang, Y.; Lu, X.; Lin, Y. Selenium Heterocyclic Electron Acceptor with Small Urbach Energy for As-Cast High-Performance Organic Solar Cells. *J. Am. Chem. Soc.* **2020**, *142*, 18741–18745. [[CrossRef](#)]
30. Liu, Q.; Jiang, Y.; Jin, K.; Qin, J.; Xu, J.; Li, W.; Xiong, J.; Liu, J.; Xiao, Z.; Sun, K.; et al. 18% Efficiency organic solar cells. *Sci. Bull.* **2020**, *65*, 272–275. [[CrossRef](#)]
31. Li, C.; Zhou, J.; Song, J.; Xu, J.; Zhang, H.; Zhang, X.; Guo, J.; Zhu, L.; Wei, D.; Han, G.; et al. Non-fullerene acceptors with branched side chains and improved molecular packing to exceed 18% efficiency in organic solar cells. *Nat. Energy* **2021**, *6*, 605–613. [[CrossRef](#)]
32. Jin, K.; Xiao, Z.; Ding, L. D18, an eximious solar polymer! *J. Semicond.* **2021**, *42*. [[CrossRef](#)]
33. Lin, Y.; Adilbekova, B.; Firdaus, Y.; Yengel, E.; Faber, H.; Sajjad, M.; Zheng, X.; Yarali, E.; Seitkhan, A.; Bakr, O.M.; et al. 17% Efficient Organic Solar Cells Based on Liquid Exfoliated WS₂ as a Replacement for PEDOT:PSS. *Adv. Mater.* **2019**, *31*, 1902965. [[CrossRef](#)] [[PubMed](#)]
34. Li, D.; Zhu, L.; Liu, X.; Xiao, W.; Yang, J.; Ma, R.; Ding, L.; Liu, F.; Duan, C.; Fahlman, M.; et al. Enhanced and Balanced Charge Transport Boosting Ternary Solar Cells Over 17% Efficiency. *Adv. Mater.* **2020**, *32*, 2002344. [[CrossRef](#)] [[PubMed](#)]
35. Lin, Y.; Firdaus, Y.; Nugraha, M.I.; Liu, F.; Karuthedath, S.; Emwas, A.; Zhang, W.; Seitkhan, A.; Neophytou, M.; Faber, H.; et al. 17.1% Efficient Single-Junction Organic Solar Cells Enabled by n-Type Doping of the Bulk-Heterojunction. *Adv. Sci.* **2020**, *7*, 1903419. [[CrossRef](#)]
36. Cui, M.; Li, D.; Du, X.; Li, N.; Rong, Q.; Li, N.; Shui, L.; Zhou, G.; Wang, X.; Brabec, C.J.; et al. A Cost-Effective, Aqueous-Solution-Processed Cathode Interlayer Based on Organosilica Nanodots for Highly Efficient and Stable Organic Solar Cells. *Adv. Mater.* **2020**, *32*, 2002973. [[CrossRef](#)]
37. Sun, R.; Wang, W.; Yu, H.; Chen, Z.; Xia, X.; Shen, H.; Guo, J.; Shi, M.; Zheng, Y.; Wu, Y.; et al. Achieving over 17% efficiency of ternary all-polymer solar cells with two well-compatible polymer acceptors. *Joule* **2021**, *5*, 1548–1565. [[CrossRef](#)]
38. An, Q.; Wang, J.; Gao, W.; Ma, X.; Hu, Z.; Gao, J.; Xu, C.; Hao, M.; Zhang, X.; Yang, C.; et al. Alloy-like ternary polymer solar cells with over 17.2% efficiency. *Sci. Bull.* **2020**, *65*, 538–545. [[CrossRef](#)]
39. Ma, X.; Wang, J.; Gao, J.; Hu, Z.; Xu, C.; Zhang, X.L.; Zhang, F. Achieving 17.4% Efficiency of Ternary Organic Photovoltaics with Two Well-Compatible Nonfullerene Acceptors for Minimizing Energy Loss. *Adv. Energy Mater.* **2020**, *10*, 2001404. [[CrossRef](#)]
40. Ma, R.; Liu, T.; Luo, Z.; Gao, K.; Chen, K.; Zhang, G.; Gao, W.; Xiao, Y.; Lau, T.-K.; Fan, Q.; et al. Adding a Third Component with Reduced Miscibility and Higher LUMO Level Enables Efficient Ternary Organic Solar Cells. *ACS Energy Lett.* **2020**, *5*, 2711–2720. [[CrossRef](#)]

41. Li, S.; Zhan, L.; Jin, Y.; Zhou, G.; Lau, T.; Qin, R.; Shi, M.; Li, C.; Zhu, H.; Lu, X.; et al. Asymmetric Electron Acceptors for High-Efficiency and Low-Energy-Loss Organic Photovoltaics. *Adv. Mater.* **2020**, *32*, 2001160. [[CrossRef](#)]
42. Ma, Q.; Jia, Z.; Meng, L.; Zhang, J.; Zhang, H.; Huang, W.; Yuan, J.; Gao, F.; Wan, Y.; Zhang, Z.; et al. Promoting charge separation resulting in ternary organic solar cells efficiency over 17.5%. *Nano Energy* **2020**, *78*, 105272. [[CrossRef](#)]
43. An, Q.; Wang, J.; Ma, X.; Gao, J.; Hu, Z.; Liu, B.; Sun, H.; Guo, X.; Zhang, X.L.; Zhang, F. Two compatible polymer donors contribute synergistically for ternary organic solar cells with 17.53% efficiency. *Energy Environ. Sci.* **2020**, *13*, 5039–5047. [[CrossRef](#)]
44. Wang, X.; Sun, Q.; Gao, J.; Ma, X.; Son, J.H.; Jeong, S.Y.; Hu, Z.; Niu, L.; Woo, H.Y.; Zhang, J.; et al. Ternary Organic Photovoltaic Cells Exhibiting 17.59% Efficiency with Two Compatible Y6 Derivations as Acceptor. *Sol. RRL* **2021**, *5*, 2100007. [[CrossRef](#)]
45. Chen, Y.; Bai, F.; Peng, Z.; Zhu, L.; Zhang, J.; Zou, X.; Qin, Y.; Kim, H.K.; Yuan, J.; Ma, L.; et al. Asymmetric Alkoxy and Alkyl Substitution on Nonfullerene Acceptors Enabling High-Performance Organic Solar Cells. *Adv. Energy Mater.* **2020**, *11*, 2003141. [[CrossRef](#)]
46. Gao, J.; Ma, X.; Xu, C.; Wang, X.; Son, J.H.; Jeong, S.Y.; Zhang, Y.; Zhang, C.; Wang, K.; Niu, L.; et al. Over 17.7% efficiency ternary-blend organic solar cells with low energy-loss and good thickness-tolerance. *Chem. Eng. J.* **2022**, *428*, 129276. [[CrossRef](#)]
47. Ma, X.; Zeng, A.; Gao, J.; Hu, Z.; Xu, C.; Son, J.H.; Jeong, S.Y.; Zhang, C.; Li, M.; Wang, K.; et al. Approaching 18% efficiency of ternary organic photovoltaics with wide bandgap polymer donor and well compatible Y6: Y6-1O as acceptor. *Natl. Sci. Rev.* **2021**, *8*, nwa305. [[CrossRef](#)]
48. Lin, Y.; Nugraha, M.I.; Firdaus, Y.; Scaccabarozzi, A.D.; Anies, F.; Emwas, A.-H.; Yengel, E.; Zheng, X.; Liu, J.; Wahyudi, W.; et al. A Simple n-Dopant Derived from Diquat Boosts the Efficiency of Organic Solar Cells to 18.3%. *ACS Energy Lett.* **2020**, *5*, 3663–3671. [[CrossRef](#)]
49. Ye, F.; Yang, W.; Luo, D.; Zhu, R.; Gong, Q. Applications of cesium in the perovskite solar cells. *J. Semicond.* **2017**, *38*, 011003. [[CrossRef](#)]
50. Li, K.; Wu, Y.; Li, X.; Fu, H.; Zhan, C. 17.1%-Efficiency organic photovoltaic cell enabled with two higher-LUMO-level acceptor guests as the quaternary strategy. *Sci. China Chem.* **2020**, *63*, 490–496. [[CrossRef](#)]
51. Zhang, W.; Huang, J.; Xu, J.; Han, M.; Su, D.; Wu, N.; Zhang, C.; Xu, A.; Zhan, C. Phthalimide Polymer Donor Guests Enable over 17% Efficient Organic Solar Cells via Parallel-Like Ternary and Quaternary Strategies. *Adv. Energy Mater.* **2020**, *10*, 2001436. [[CrossRef](#)]
52. Li, X.; Zhou, L.; Lu, X.; Cao, L.; Du, X.; Lin, H.; Zheng, C.; Tao, S. Hydrogen bond induced high-performance quaternary organic solar cells with efficiency up to 17.48% and superior thermal stability. *Mater. Chem. Front.* **2021**, *5*, 3850–3858. [[CrossRef](#)]
53. Arunagiri, L.; Peng, Z.; Zou, X.; Yu, H.; Zhang, G.; Wang, Z.; Lai, J.Y.L.; Zhang, J.; Zheng, Y.; Cui, C.; et al. Selective Hole and Electron Transport in Efficient Quaternary Blend Organic Solar Cells. *Joule* **2020**, *4*, 1790–1805. [[CrossRef](#)]
54. Zhang, M.; Zhu, L.; Zhou, G.; Hao, T.; Qiu, C.; Zhao, Z.; Hu, Q.; Larson, B.W.; Zhu, H.; Ma, Z.; et al. Single-layered organic photovoltaics with double cascading charge transport pathways: 18% efficiencies. *Nat. Commun.* **2021**, *12*, 309. [[CrossRef](#)]
55. Cui, Y.; Yao, H.; Zhang, J.; Zhang, T.; Wang, Y.; Hong, L.; Xian, K.; Xu, B.; Zhang, S.; Peng, J.; et al. Over 16% efficiency organic photovoltaic cells enabled by a chlorinated acceptor with increased open-circuit voltages. *Nat. Commun.* **2019**, *10*, 2515. [[CrossRef](#)]
56. Hong, L.; Yao, H.; Wu, Z.; Cui, Y.; Zhang, T.; Xu, Y.; Yu, R.; Liao, Q.; Gao, B.; Xian, K.; et al. Eco-Compatible Solvent-Processed Organic Photovoltaic Cells with Over 16% Efficiency. *Adv. Mater.* **2019**, *31*, 1903441. [[CrossRef](#)]
57. Chen, H.; Lai, H.; Chen, Z.; Zhu, Y.; Wang, H.; Han, L.; Zhang, Y.; He, F. 17.1 %-Efficient Eco-Compatible Organic Solar Cells from a Dissymmetric 3D Network Acceptor. *Angew. Chem. Int. Ed.* **2021**, *60*, 3238–3246. [[CrossRef](#)] [[PubMed](#)]
58. Zhang, M.; Guo, X.; Ma, W.; Ade, H.; Hou, J. A Large-Bandgap Conjugated Polymer for Versatile Photovoltaic Applications with High Performance. *Adv. Mater.* **2015**, *27*, 4655–4660. [[CrossRef](#)]
59. Hu, Z.; Yang, L.; Gao, W.; Gao, J.; Xu, C.; Zhang, X.L.; Wang, Z.; Tang, W.; Yang, C.; Zhang, F. Over 15.7% Efficiency of Ternary Organic Solar Cells by Employing Two Compatible Acceptors with Similar LUMO Levels. *Small* **2020**, *16*, 2000441. [[CrossRef](#)]
60. Zhang, S.; Qin, Y.; Zhu, J.; Hou, J. Over 14% Efficiency in Polymer Solar Cells Enabled by a Chlorinated Polymer Donor. *Adv. Mater.* **2018**, *30*, 1800868. [[CrossRef](#)]
61. Fan, B.; Zhang, D.; Li, M.; Zhong, W.; Zeng, Z.; Ying, L.; Huang, F.; Cao, Y. Achieving over 16% efficiency for single-junction organic solar cells. *Sci. China Chem.* **2019**, *62*, 746–752. [[CrossRef](#)]
62. Xiong, J.; Jin, K.; Jiang, Y.; Qin, J.; Wang, T.; Liu, J.; Liu, Q.; Peng, H.; Li, X.; Sun, A.; et al. Thiolactone copolymer donor gifts organic solar cells a 16.72% efficiency. *Sci. Bull.* **2019**, *64*, 1573–1576. [[CrossRef](#)]
63. Xu, X.; Feng, K.; Bi, Z.; Ma, W.; Zhang, G.; Peng, Q. Single-Junction Polymer Solar Cells with 16.35% Efficiency Enabled by a Platinum(II) Complexation Strategy. *Adv. Mater.* **2019**, *31*, 1901872. [[CrossRef](#)] [[PubMed](#)]
64. Zhang, M.; Xiao, Z.; Gao, W.; Liu, Q.; Jin, K.; Wang, W.; Mi, Y.; An, Q.; Ma, X.; Liu, X.; et al. Over 13% Efficiency Ternary Nonfullerene Polymer Solar Cells with Tilted Up Absorption Edge by Incorporating a Medium Bandgap Acceptor. *Adv. Energy Mater.* **2018**, *8*, 1801968. [[CrossRef](#)]
65. Zhao, Z.; Li, C.; Shen, L.; Zhang, X.; Zhang, F. Photomultiplication type organic photodetectors based on electron tunneling injection. *Nanoscale* **2020**, *12*, 1091–1099. [[CrossRef](#)]
66. Du, X.; Yuan, Y.; Zhou, L.; Lin, H.; Zheng, C.; Luo, J.; Chen, Z.; Tao, S.; Liao, L. Delayed Fluorescence Emitter Enables Near 17% Efficiency Ternary Organic Solar Cells with Enhanced Storage Stability and Reduced Recombination Energy Loss. *Adv. Funct. Mater.* **2020**, *30*, 1909837. [[CrossRef](#)]

67. Ma, X.; Gao, W.; Yu, J.; An, Q.; Zhang, M.; Hu, Z.; Wang, J.; Tang, W.; Yang, C.; Zhang, F. Ternary nonfullerene polymer solar cells with efficiency >13.7% by integrating the advantages of the materials and two binary cells. *Energy Environ. Sci.* **2018**, *11*, 2134–2141. [[CrossRef](#)]
68. Yan, T.; Ge, J.; Lei, T.; Zhang, W.; Song, W.; Fanady, B.; Zhang, D.; Chen, S.; Peng, R.; Ge, Z. 16.55% efficiency ternary organic solar cells enabled by incorporating a small molecular donor. *J. Mater. Chem. A* **2019**, *7*, 25894–25899. [[CrossRef](#)]
69. An, Q.; Zhang, F.; Zhang, J.; Tang, W.; Deng, Z.; Hu, B. Versatile ternary organic solar cells: A critical review. *Energy Environ. Sci.* **2016**, *9*, 281–322. [[CrossRef](#)]
70. Chen, S.; Yan, T.; Fanady, B.; Song, W.; Ge, J.; Wei, Q.; Peng, R.; Chen, G.; Zou, Y.; Ge, Z. High efficiency ternary organic solar cells enabled by compatible dual-donor strategy with planar conjugated structures. *Sci. China Chem.* **2020**, *63*, 917–923. [[CrossRef](#)]
71. Wang, Y.; Wang, F.; Gao, J.; Yan, Y.; Wang, X.; Wang, X.; Xu, C.; Ma, X.; Zhang, J.; Zhang, F. Organic photovoltaics with 300 nm thick ternary active layer exhibiting 15.6% efficiency. *J. Mater. Chem. C* **2021**, *9*. [[CrossRef](#)]
72. Jiang, H.; Li, X.; Wang, J.; Qiao, S.; Zhang, Y.; Zheng, N.; Chen, W.; Li, Y.; Yang, R. Ternary Polymer Solar Cells with High Efficiency of 14.24% by Integrating Two Well-Complementary Nonfullerene Acceptors. *Adv. Funct. Mater.* **2019**, *29*, 1903596. [[CrossRef](#)]
73. Zhang, M.; Gao, W.; Zhang, F.; Mi, Y.; Wang, W.; An, Q.; Wang, J.; Ma, X.; Miao, J.; Hu, Z.; et al. Efficient ternary non-fullerene polymer solar cells with PCE of 11.92% and FF of 76.5%. *Energy Environ. Sci.* **2018**, *11*, 841–849. [[CrossRef](#)]
74. Liu, M.; Wang, J.; Zhao, Z.; Yang, K.; Durand, P.; Ceugniet, F.; Ulrich, G.; Niu, L.; Ma, Y.; Leclerc, N.; et al. Ultra-Narrow-Band NIR Photomultiplication Organic Photodetectors Based on Charge Injection Narrowing. *J. Phys. Chem. Lett.* **2021**, *12*, 2937–2943. [[CrossRef](#)] [[PubMed](#)]
75. Cheng, P.; Liu, Y.; Chang, S.-Y.; Li, T.; Sun, P.; Wang, R.; Cheng, H.-W.; Huang, T.; Meng, L.; Nuryyeva, S.; et al. Efficient Tandem Organic Photovoltaics with Tunable Rear Sub-cells. *Joule* **2019**, *3*, 432–442. [[CrossRef](#)]
76. Ma, X.; An, Q.; Ibraikulov, O.; Lévêque, P.; Heiser, T.; Leclerc, N.; Zhang, X.; Zhang, F. Efficient ternary organic photovoltaics with two polymer donors by minimizing energy loss. *J. Mater. Chem. A* **2020**, *8*, 1265–1272. [[CrossRef](#)]
77. Jiang, K.; Wei, Q.; Lai, J.Y.L.; Peng, Z.; Kim, H.K.; Yuan, J.; Ye, L.; Ade, H.; Zou, Y.; Yan, H. Alkyl Chain Tuning of Small Molecule Acceptors for Efficient Organic Solar Cells. *Joule* **2019**, *3*, 3020–3033. [[CrossRef](#)]
78. Ma, X.; Luo, M.; Gao, W.; Yuan, J.; An, Q.; Zhang, M.; Hu, Z.; Gao, J.; Wang, J.; Zou, Y.; et al. Achieving 14.11% efficiency of ternary polymer solar cells by simultaneously optimizing photon harvesting and exciton distribution. *J. Mater. Chem. A* **2019**, *7*, 7843–7851. [[CrossRef](#)]
79. Zhao, Z.; Wang, J.; Xu, C.; Yang, K.; Zhao, F.; Wang, K.; Zhang, X.L.; Zhang, F. Photomultiplication Type Broad Response Organic Photodetectors with One Absorber Layer and One Multiplication Layer. *J. Phys. Chem. Lett.* **2020**, *11*, 366–373. [[CrossRef](#)]
80. Yan, C.; Tang, H.; Ma, R.; Zhang, M.; Liu, T.; Lv, J.; Huang, J.; Yang, Y.; Xu, T.; Kan, Z.; et al. Synergy of Liquid-Crystalline Small-Molecule and Polymeric Donors Delivers Uncommon Morphology Evolution and 16.6% Efficiency Organic Photovoltaics. *Adv. Sci.* **2020**, *7*, 2000149. [[CrossRef](#)]
81. Xu, C.; Chen, H.; Zhao, Z.; Gao, J.; Ma, X.; Lu, S.; Zhang, X.; Xiao, Z.; Zhang, F. 14.46% Efficiency small molecule organic photovoltaics enabled by the well trade-off between phase separation and photon harvesting. *J. Energy Chem.* **2021**, *57*, 610–617. [[CrossRef](#)]
82. Song, J.; Li, C.; Zhu, L.; Guo, J.; Xu, J.; Zhang, X.; Weng, K.; Zhang, K.; Min, J.; Hao, X.; et al. Ternary Organic Solar Cells with Efficiency >16.5% Based on Two Compatible Nonfullerene Acceptors. *Adv. Mater.* **2019**, *31*, 1905645. [[CrossRef](#)] [[PubMed](#)]
83. Zhao, Z.; Liu, B.; Xu, C.; Liu, M.; Yang, K.; Zhang, X.L.; Xu, Y.; Zhang, J.; Li, W.; Zhang, F. Highly sensitive all-polymer photodetectors with ultraviolet-visible to near-infrared photo-detection and their application as an optical switch. *J. Mater. Chem. C* **2021**, *9*, 5349–5355. [[CrossRef](#)]
84. Lu, L.; Kelly, M.A.; You, W.; Yu, L. Status and prospects for ternary organic photovoltaics. *Nat. Photon.* **2015**, *9*, 491–500. [[CrossRef](#)]
85. An, Q.; Zhang, F.; Gao, W.; Sun, Q.; Zhang, M.; Yang, C.; Zhang, J. High-efficiency and air stable fullerene-free ternary organic solar cells. *Nano Energy* **2018**, *45*, 177–183. [[CrossRef](#)]
86. Mohapatra, A.A.; Kim, V.; Puttaraju, B.; Sadhanala, A.; Jiao, X.; McNeill, C.R.; Friend, R.H.; Patil, S. Förster Resonance Energy Transfer Drives Higher Efficiency in Ternary Blend Organic Solar Cells. *ACS Appl. Energy Mater.* **2018**, *1*, 4874–4882. [[CrossRef](#)]
87. Yang, K.; Wang, J.; Zhao, Z.; Zhou, Z.; Liu, M.; Zhang, J.; He, Z.; Zhang, F. Smart Strategy: Transparent Hole-Transporting Polymer as a Regulator to Optimize Photomultiplication-type Polymer Photodetectors. *ACS Appl. Mater. Interfaces* **2021**, *13*, 21565–21572. [[CrossRef](#)]
88. Yang, L.; Yan, L.; You, W. Organic Solar Cells beyond One Pair of Donor–Acceptor: Ternary Blends and More. *J. Phys. Chem. Lett.* **2013**, *4*, 1802–1810. [[CrossRef](#)] [[PubMed](#)]
89. Zhan, L.; Li, S.; Lau, T.-K.; Cui, Y.; Lu, X.; Shi, M.; Li, C.-Z.; Li, H.; Hou, J.; Chen, H. Over 17% efficiency ternary organic solar cells enabled by two non-fullerene acceptors working in an alloy-like model. *Energy Environ. Sci.* **2020**, *13*, 635–645. [[CrossRef](#)]
90. Fu, H.; Wang, Z.; Sun, Y. Advances in Non-Fullerene Acceptor Based Ternary Organic Solar Cells. *Sol. RRL* **2018**, *2*, 1700158. [[CrossRef](#)]
91. Yang, K.; Wang, J.; Zhao, Z.; Zhao, F.; Wang, K.; Zhang, X.; Zhang, F. Ultraviolet to near-infrared broadband organic photodetectors with photomultiplication. *Org. Electron.* **2020**, *83*, 105739. [[CrossRef](#)]
92. Hu, Z.; Wang, J.; Ma, X.; Gao, J.; Xu, C.; Wang, X.; Zhang, X.; Wang, Z.; Zhang, F. Semitransparent organic solar cells exhibiting 13.02% efficiency and 20.2% average visible transmittance. *J. Mater. Chem. A* **2021**, *9*, 6797–6804. [[CrossRef](#)]

93. Li, D.; Chen, X.; Cai, J.; Li, W.; Chen, M.; Mao, Y.; Du, B.; Smith, J.; Kilbride, R.C.; O’Kane, M.E.; et al. Non-fullerene acceptor fibrils enable efficient ternary organic solar cells with 16.6% efficiency. *Sci. China Chem.* **2020**, *63*, 1461–1468. [[CrossRef](#)]
94. Gao, J.; Wang, J.; An, Q.; Ma, X.; Hu, Z.; Xu, C.; Zhang, X.; Zhang, F. Over 16.7% efficiency of ternary organic photovoltaics by employing extra PC71BM as morphology regulator. *Sci. China Chem.* **2019**, *63*, 83–91. [[CrossRef](#)]
95. Jiang, M.; Bai, H.; Zhi, H.; Yan, L.; Woo, H.Y.; Tong, L.; Wang, J.; Zhang, F.; An, Q. Rational compatibility in a ternary matrix enables all-small-molecule organic solar cells with over 16% efficiency. *Energy Environ. Sci.* **2021**, *14*, 3945–3953. [[CrossRef](#)]
96. Yan, T.; Song, W.; Huang, J.; Peng, R.; Huang, L.; Ge, Z. 16.67% Rigid and 14.06% Flexible Organic Solar Cells Enabled by Ternary Heterojunction Strategy. *Adv. Mater.* **2019**, *31*, 1902210. [[CrossRef](#)]
97. Luo, Z.; Sun, R.; Zhong, C.; Liu, T.; Zhang, G.; Zou, Y.; Jiao, X.; Min, J.; Yang, C. Altering alkyl-chains branching positions for boosting the performance of small-molecule acceptors for highly efficient nonfullerene organic solar cells. *Sci. China Chem.* **2020**, *63*, 361–369. [[CrossRef](#)]
98. Chang, Y.; Lau, T.-K.; Pan, M.-A.; Lu, X.; Yan, H.; Zhan, C. The synergy of host–guest nonfullerene acceptors enables 16%-efficiency polymer solar cells with increased open-circuit voltage and fill-factor. *Mater. Horizons* **2019**, *6*, 2094–2102. [[CrossRef](#)]
99. Menke, S.M.; Ran, N.A.; Bazan, G.C.; Friend, R.H. Understanding Energy Loss in Organic Solar Cells: Toward a New Efficiency Regime. *Joule* **2018**, *2*, 25–35. [[CrossRef](#)]
100. Yu, R.; Yao, H.; Cui, Y.; Hong, L.; He, C.; Hou, J. Improved Charge Transport and Reduced Nonradiative Energy Loss Enable Over 16% Efficiency in Ternary Polymer Solar Cells. *Adv. Mater.* **2019**, *31*, 1902302. [[CrossRef](#)]
101. Ma, X.; Wang, J.; An, Q.; Gao, J.; Hu, Z.; Xu, C.; Zhang, X.; Liu, Z.; Zhang, F. Highly efficient quaternary organic photovoltaics by optimizing photogenerated exciton distribution and active layer morphology. *Nano Energy* **2020**, *70*, 20104496. [[CrossRef](#)]
102. Guillemoles, J.-F.; Kirchartz, T.; Cahen, D.; Rau, U. Guide for the perplexed to the Shockley–Queisser model for solar cells. *Nat. Photon.* **2019**, *13*, 501–505. [[CrossRef](#)]
103. Liu, M.; Wang, J.; Yang, K.; Zhao, Z.; Zhou, Z.; Ma, Y.; Shen, L.; Ma, X.; Zhang, F. Highly sensitive, broad-band organic photomultiplication-type photodetectors covering UV-Vis-NIR. *J. Mater. Chem. C* **2021**, *9*, 6357–6364. [[CrossRef](#)]
104. Meng, L.; Zhang, Y.; Wan, X.; Li, C.; Zhang, X.; Wang, Y.; Ke, X.; Xiao, Z.; Ding, L.; Xia, R. Organic and solution-processed tandem solar cells with 17.3% efficiency. *Science* **2018**, *361*, 1094–1098. [[CrossRef](#)] [[PubMed](#)]
105. Hu, Z.; Wang, J.; Ma, X.; Gao, J.; Xu, C.; Yang, K.; Wang, Z.; Zhang, J.; Zhang, F. A critical review on semitransparent organic solar cells. *Nano Energy* **2020**, *78*, 20105376. [[CrossRef](#)]
106. Ho, C.H.Y.; Kim, T.; Xiong, Y.; Firdaus, Y.; Yi, X.; Dong, Q.; Rech, J.J.; Gadisa, A.; Booth, R.; O’Connor, B.T.; et al. High-Performance Tandem Organic Solar Cells Using HSolar as the Interconnecting Layer. *Adv. Energy Mater.* **2020**, *10*, 2000823. [[CrossRef](#)]
107. Liu, G.; Xia, R.; Huang, Q.; Zhang, K.; Hu, Z.; Jia, T.; Liu, X.; Yip, H.; Huang, F. Tandem Organic Solar Cells with 18.7% Efficiency Enabled by Suppressing the Charge Recombination in Front Sub-Cell. *Adv. Funct. Mater.* **2021**, *31*, 2103283. [[CrossRef](#)]
108. Chen, W.; Sun, H.; Hu, Q.; Djurišić, A.B.; Russell, T.P.; Guo, X.; He, Z. High Short-Circuit Current Density via Integrating the Perovskite and Ternary Organic Bulk Heterojunction. *ACS Energy Lett.* **2019**, *4*, 2535–2536. [[CrossRef](#)]
109. Zhao, Z.; Liu, B.; Xie, C.; Ma, Y.; Wang, J.; Liu, M.; Yang, K.; Xu, Y.; Zhang, J.; Li, W. Highly sensitive, sub-microsecond polymer photodetectors for blood oxygen saturation testing. *Sci. China Chem.* **2021**, *64*. [[CrossRef](#)]
110. Zeng, M.; Wang, X.; Ma, R.; Zhu, W.; Li, Y.; Chen, Z.; Zhou, J.; Li, W.; Liu, T.; He, Z.; et al. Dopamine Semiquinone Radical Doped PEDOT:PSS: Enhanced Conductivity, Work Function and Performance in Organic Solar Cells. *Adv. Energy Mater.* **2020**, *10*, 2000743. [[CrossRef](#)]
111. Kang, Q.; Zheng, Z.; Zu, Y.; Liao, Q.; Bi, P.; Zhang, S.; Yang, Y.; Xu, B.; Hou, J. n-doped inorganic molecular clusters as a new type of hole transport material for efficient organic solar cells. *Joule* **2021**, *5*, 646–658. [[CrossRef](#)]
112. Lin, Y.; Magomedov, A.; Firdaus, Y.; Kaltsas, D.; El-Labban, A.; Faber, H.; Naphade, D.R.; Yengel, E.; Zheng, X.; Yarali, E.; et al. 18.4% Organic Solar Cells Using a High Ionization Energy Self-Assembled Monolayer as Hole-Extraction Interlayer. *ChemSusChem* **2021**, 2100707. [[CrossRef](#)] [[PubMed](#)]